

DEVELOPING THE DESIGN OF ROAD GOING WELDED STRUCTURES WITH SPECIAL
CONSIDERATIONS FOR HOT-DIP GALVANIZING

By

Daniel Landgraf

Mohammad Mahtabi
Assistant Professor of Engineering
(Major Advisor, Chair)

Hamdy Ibrahim
Assistant Professor of Engineering
(Committee Member)

Louie Elliott
Assistant Professor of Engineering
(Committee Member)

DEVELOPING THE DESIGN OF ROAD GOING WELDED STRUCTURES WITH SPECIAL
CONSIDERATIONS FOR HOT-DIP GALVANIZING

By

Daniel Landgraf

A Thesis Submitted to the Faculty of the University of
Tennessee at Chattanooga in Partial
Fulfillment of the Requirements of the Degree
of Master of Science: Engineering

The University of Tennessee at Chattanooga
Chattanooga, Tennessee

December 2019

ABSTRACT

The primary objective of this thesis is to provide accessible methods for numerical analysis of the mechanical behavior of welded structures specific to roadgoing trailers as defined by the Federal Motor Carrier Safety Administration. The area of highest interest is hot-dip galvanizing. The influence of temperature on steel has long been studied and several sources have found, or otherwise mathematical expressions were derived which describe the relationships between mechanical properties and temperature. Understanding all failure modes associated with the design of a structurally acceptable trailer goes beyond a simple static force analysis. Road going trailers undergo acceleration in the vertical, lateral, fore and aft directions sometimes in excess of three times the acceleration of gravity. Additionally, in the case of traversing uneven terrain, these loads can become cyclical and therefore, fatigue must be taken into consideration. This paper represents a proposed guideline for structural design.

ACKNOWLEDGEMENTS

Standing precariously on the shoulders of giants, I am humbly grateful to all those before me and presumptuously thankful to all those after me. Special thanks to Sherman + Reilly, Inc., specifically, Doug MacDonald and Matthew Faircloth, and to my academic advisors: Dr. Damshala and Dr. Mahtabi. Thank you, also, to my parents, Hank and Ellen Landgraf for their continued support. Much appreciation goes to Valmont Coatings and its employees at the facility in Steele, Alabama for assistance in my research of hot-dip galvanizing. Finally, thank you to committee members for their time in reviewing this document.

EXECUTIVE SUMMARY

This thesis emphasizes a method of design by analysis where the design criteria is determined directly from a stress analysis used to determine maximum allowable loads. Load cases are developed and analyzed by use of strategic assumptions to idealize the actual conditions in the most accurate way possible. Although some analytical methods are presented, numerical and finite element methods are preferable due to their inherent accessibility. Because of the specific nature of the analysis herein, no failure criterion is specified. Although the von Mises yield criterion is heavily used in finite element software due to its curve continuity, in cases of uncertainty, the Tresca yield criterion is certainly acceptable as it lends itself to being more conservative.

In the winter of 2018, a custom trailer being hot-dipped galvanized, suffered an unexpected material failure during the dipping process. It was determined at the time that the failure was caused by joint stiffness restricting the thermal expansion effects which, in turn, produced adequate stresses to ultimately fracture the material. This work represents an investigation into the root cause of the failure and proposes methods of predictive analysis to prevent such failures in the future. The conclusion of the analysis indicate that material property and joint restriction dominate structural integrity at elevated temperatures. The trailer was redesigned in accordance with these methods and was successfully dipped without failure in the summer of 2019.

TABLE OF CONTENTS

ABSTRACT.....	iii
ACKNOWLEDGEMENTS.....	iv
EXECUTIVE SUMMARY	v
TABLE OF CONTENTS.....	vi
LIST OF TABLES.....	ix
LIST OF FIGURES	x
LIST OF ABBREVIATIONS.....	xii
LIST OF SYMBOLS	xiii
CHAPTER	
1. INTRODUCTION	1
1.1 Trailer Design for Utility Equipment.....	1
2. REVIEW OF CONCEPTS AND LITERATURE	5
2.1 Brief Mention of Stress and Strain.....	5
2.2 Failure and Fatigue	7
2.2.1 Mechanical Fatigue.....	7
2.2.2 Methods for Analysis of Failure	8
2.2.3 Method for Estimating Fatigue Life	11
2.3 Welded Joint Design.....	13
2.3.1 Stress Analysis.....	13
Tensile or Compressive Load Case.....	15
Shear Load Case	15
Allowable Stress	16
Fillet Weld Strength.....	16
2.3.2 Weldability.....	16
2.3.3 Considerations for Pre-Heating and Base Material Selection.....	18
Zone I.....	18

Zone II.....	18
Zone III	20
2.4 Material Analysis	22
2.4.1 Material Selection	22
Material Shapes.....	22
2.4.2 Mechanical Properties, Behavior and Preferences.....	24
Brief Note on Metal Forming	24
Material Preferences	26
Tensile Requirements.....	28
Chemical Limitations.....	30
2.5 Thermal Considerations	31
2.5.1 Topics on Galvanizing	31
Introduction to Galvanizing and Its Purpose in Industry	31
Brief Weight Gain Discussion	34
Discussion on Hydrogen Embrittlement.....	37
2.6 Discussion of Material Properties at Elevated Temperatures	39
2.6.1 Steel at Elevated Temperatures.....	39
Mechanical Properties of Steel at Elevated Temperatures	39
Thermophysical Properties of Steel at Elevated Temperatures	43
2.6.2 Zinc at Elevated Temperatures	45
Thermophysical Properties of Zinc at Elevated Temperatures	45
2.7 Determination of a Convection Coefficient.....	47
2.7.1 Free Convection	47
2.8 Theoretical Solutions to Thermal Analysis.....	49
2.8.1 Constant Surface Convection.....	49
2.8.2 Constant Surface Temperature.....	50
2.8.3 Exact and Approximate Solutions to Transient Conduction.....	51
2.8.4 Sample Finite Element Thermal Analysis	53
Transient Study with Free Convection Using Finite Element Analysis	
Software	53
Sample Solution for Constant Surface Convection	54
Application of Concepts	54
3. FINITE ELEMENT ANALYSIS OF A NEW DESIGN.....	56
3.1 Design for Hot-Dip Galvanizing.....	56
3.1.1 Design Logic	56
3.1.2 Design Comparison.....	57
3.1.3 Thermal Analysis of Designs.....	59
4. CONCLUSIONS AND FUTURE WORK.....	68
REFERENCES	70
APPENDIX	

A. RELEVANT PROPERTIES OF LOAD BEARING MEMBERS	75
B. IMPORTANT LOAD CONSIDERATIONS	82
C. INSTRUMENTATION	87
VITA.....	95

LIST OF TABLES

2.1	Susceptibility index rating	21
2.2	Minimum preheat and inter-pass temperatures °F [15]	21
2.3	Tensile requirements of a few common steels [25] [26] [27]	29
2.4	Collected average values for common steels	30
2.5	Chemical composition as a percentage of typical steels [25] [26] [27]	31
2.6	Coating thickness and weight [32]	35
2.7	Tabulated values of C_n and ζ_n	52

LIST OF FIGURES

1.1	An example of material failure during hot-dip galvanizing (Shared with Permission from Sherman + Reilly, Inc.)	3
1.2	Analysis showing stresses in a structure with high restraint	4
2.1	Effect of strain rate and temperature on fracture toughness [7].....	10
2.2	Relationship between Rockwell hardness and UTS	12
2.3	Representation of alteration in base material grain structure near a welded joint [10]	13
2.4	HAZ of a fillet weld.....	14
2.5	Reference figure for stress analysis showing weld parameters	14
2.6	Reference directions for welded joints [7].....	15
2.7	Zone classification of steels [15]	18
2.8	Critical Cooling Rates (CCR) based on CE [15]	19
2.9	Cooling rate based on energy input and joint geometry [15].....	20
2.10	Typical forming visual description [23]	25
2.11	Preferential use of materials for structural shapes	27
2.12	Preferential use of materials for plates and bars	28
2.13	Sample certified mill test report for A572 grade 50 steel W-shapes	29
2.14	Effects of zinc additives to galvanized materials [29]	33
2.15	Micrograph of LMAC caused by infiltration of galvanizing bath constituents into the base material [1].....	34
2.16	Typical Sandelin curve comparing coating thickness to mass percent silicon [33]	36

2.17	Galvanized coating on properly selected steel [34]	36
2.18	Galvanized coating on a Sandelin steel [34].....	37
2.19	Comparison of methods for calculating the elastic modulus verse temperature	42
2.20	Comparison of methods for calculating the yield strength verse temperature.....	42
2.21	Exact values of steel strength at elevated temperatures [38]	43
2.22	Theoretical thermophysical properties of A572 grade 50.....	44
2.23	Coefficients for density calculation	45
2.24	Temperature rise in a solid body exposed to constant surface convection	51
2.25	Result of sample FEA study	54
3.1	Simplified model of original design	58
3.2	Simplified model of new design	59
3.3	Graphic of boundary condition effects	60
3.4	Model of first design halfway dipped in galvanizing bath	61
3.5	Resulting temperature gradients from thermal study of first design.....	61
3.6	Cut section of resulting temperature gradients from thermal study of first design	62
3.7	Thermally induced stresses in first structure	63
3.8	Results from thermal study on new design.....	64
3.9	Cut section of thermal results on new design	64
3.10	Results from stress analysis on new design	65
3.11	New design post hot-dip galvanizing (shared with permission from Valmont).....	66
3.12	New design post hot-dip galvanizing (shared with permission from Valmont)	67

LIST OF ABBREVIATIONS

AISC, American Institute of Steel Construction

ASTM, American Society for Testing Materials

AWS, American Welding Society

CCR, Critical Cooling Rate

CE, Carbon Equivalent

FEA, Finite Element Analysis

FEM, Finite Element Model

FMCSA, Federal Motor Carrier Safety Administration

GAWR, Gross Axle Weight Rating

GVWR, Gross Vehicle Weight Rating

HAZ, Heat Affected Zone

HSS, Hollow Structural Section

HV, Vickers Hardness Number

LMAC, Liquid Metal Assisted Cracking

MTR, Mill Test Receipt

TR, Rectangular Tubing

UTS, Ultimate Tensile Strength

W-Beam, Wide Flanged Beam

LIST OF SYMBOLS

This thesis covers a variety of topics, each with their own commonly used symbols. As such, certain symbols herein are used in multiple instances with differing meanings. A good effort has been made to describe the symbols immediately preceding or in immediate succession of its usage. Symbols in the appendices are not listed.

A , Area or Constant, as referenced

a , Crack Size, as referenced

Bi , Biot Number

c_p , Specific Heat

\mathbb{D} , Design Factor

E , Modulus of Elasticity

F , Calculated Load or Allowable Stress, as referenced

f , Strength of Steel at Specified Temperature

Fo , Fourier Number

g , Acceleration of Gravity

Gr , Grashof Number

h , Weld Throat or Convection Coefficient

K , Stress Intensity Factor, as referenced

k , Thermal Conductivity

k' , Strength Coefficient

L , Length, as referenced

ℓ , Length, as referenced

m , Mass or Constant, as referenced

N , Susceptibility Index

N , Number of, as referenced

Nu , Nusselt Number

P , Applied Load

Pr , Prandtl Number

R , Rockwell Hardness or Weld Strength Loaded Longitudinally, as referenced

r , Radius, as referenced

RA , Percent Area Reduction

Ra , Rayleigh Number

T , Thickness or Temperature, as referenced

t , Time or Thickness, as referenced

V , Volume

w , Weld Leg Length or Beam Web, as referenced

w , Weight

Y , Geometric Factor

Z , Section Modulus

α , Linear Coefficient of Thermal Expansion or Thermal Diffusivity, as referenced

β , Volumetric Expansion Coefficient

δ , Expansion

ε , Strain, as referenced

θ , Function of Temperature, as referenced

μ , Dynamic Viscosity

ν , Poisson's Ratio, Kinematic Viscosity, as referenced

ξ , Mil Thickness

ρ , Density

σ , Stress, as referenced

τ , Shear Stress

χ , Weight per Unit Area

ϵ , True Strain

CHAPTER 1

INTRODUCTION

1.1 Trailer Design for Utility Equipment

The strategy for the design of trailers, especially those intended for heavy duty applications, cannot be summed with one simple case of analysis for there are many use cases. Basic considerations must be made for the direct loading of the vehicle and the mean environmental effects¹ during operation. A road going vehicle experiences a variety of forces exerted in multiple directions. In some instances, these forces may be singular and in others, the forces must be considered as a combined load on the vehicle.

One preference for design is to follow a set of criteria established through cases of precedent or other empirical data sets. For this method, very little is typically done to ensure the design is reaching its maximum efficiency² by the designer. Rather, the efficiency of the design is predetermined by the engineer who may or may not be in touch with the use case.

Alternatively, design criteria can be set by a general understanding of the elastic response of an assumed homogenous material whose behavior is described on the basis of just a few material

¹ This is often a topic requiring a consensus between engineers, sales representatives and product managers. In some cases, the design requirements are clear – vehicles sold only for snow plowing for example, will most likely not have to be engineered for elevated temperatures – while other times statistical models for the use case are developed to determine design criteria.

² Efficiency of a design can be measured in different ways. Generally speaking, an efficient design meets criteria set to accomplish customer, engineering, manufacturing and financial requirements.

properties. These material properties create a set of reasonable design criteria for most design requirements. Using tools such as finite element analysis software, these parameters, combined with some basic assumptions regarding the way the materials will deform and deflect under load, can be used to accurately gauge the response of structure to a prescribed load case and reasonably determine design feasibility.

There are, however, cases where these common approaches fail to truly predict a real outcome. Cases where the composition of the material is suspect, cases where the materials are subjected to boundary conditions such that the fundamental properties change as functions of said boundary parameters (such as temperature or time) and cases when the materials are strained to a point beyond their proportional limits and plastic deformation occurs, are all instances where a more in-depth analysis might be required. In these instances, special considerations have to be made to alleviate design failures. In this study, the background requirements for these considerations are discussed and special consideration is given for the analysis of welded structures during hot-dip galvanizing. An example of why it is important to make more than basic assumptions for these arguably extreme cases would be Liquid Metal Assisted Cracking (LMAC, which can be described as the response of a solid metal in contact with molten metal) in a welded structure during hot-dip galvanizing. LMAC differs from distortion or stress cracking in that it is a brittle type of fracture, while distortion cracking is usually a fatigue response to longer term exposure to stresses [1]. While the true nature of LMAC is not entirely clear, steps can be taken to reduce the likelihood of a failure occurrence. The combination of the potential for LMAC occurrence and stresses due to thermal expansion during hot-dip galvanizing require constant diligence and oversight in the design of structures for galvanizing.



Figure 1.1 An example of material failure during hot-dip galvanizing (Shared with Permission from Sherman + Reilly, Inc.)

We are able to verify the failure in this joint through theoretical methods (to be discussed later) and Finite Element Analysis (FEA) as shown in Figure 1.2 on the following page.

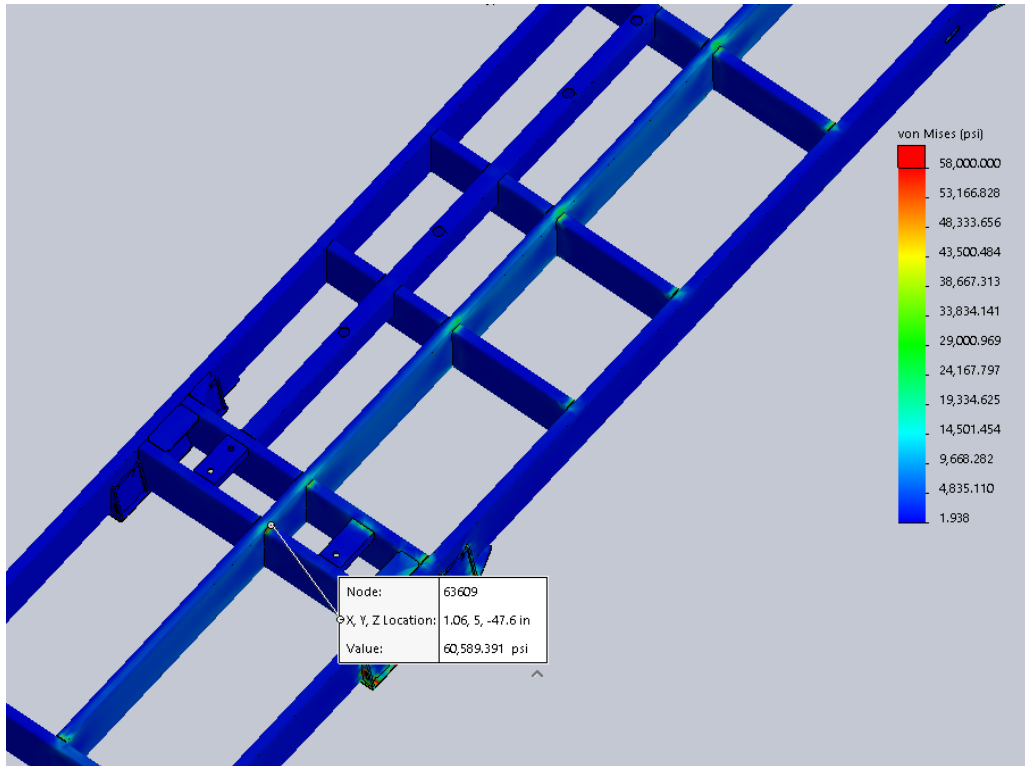


Figure 1.2 Analysis showing stresses in a structure with high restraint

The material used is ASTM A500 Grade B which has an Ultimate Tensile Strength (UTS) of 58,000 psi. We can see that the results of the analysis in Figure 1.2 show a stress more than the materials UTS and a conservative conclusion is that this structure will experience failure in this location. It is important to note that the results of any FEA are not always accurate and it is therefore important to understand what is happening from an analytical and logical perspective. An attempt is made in the ensuing pages to briefly, yet adequately cover topics and concepts which should be employed in design calculations for welded structures being hot-dip galvanized. Using this understanding, steps can be taken to reduce the failure susceptibility in high stress areas and determine if this structure can be galvanized successfully or a new design is required.

CHAPTER 2

REVIEW OF CONCEPTS AND LITERATURE

2.1 Brief Mention of Stress and Strain

Realistically, and for most engineering applications, the linear relationship between stress and strain as described by Hooke's law remains a valid tool for engineering design. One important point with respect to Hooke's law, is that the calculated stresses are average stresses as no material contains entirely perfect structure. Additionally, often only surface stresses are considered, that is a force exerted on one body surface from another body in contact; however, forces acting through the volume of the body exist as well and are aptly called, body forces. An example of stress induced from body forces are thermal stresses which quite understandably so, act through the entire volume of a body.

Typically, testing is done to measure the average linear strain experienced by a specimen and from this, the local stress is calculated. Often times, strain gauges are used for this purpose; a topic covered in the C.1 Strain Gauge Instrumentation section on page 89. This strain is given as a change in length compared with respect to some starting length of a specimen. With a linear stress-strain relationship, strain is considered as the change in length divided by the original specimen length. However, it is often more useful to look at the incremental strain. For example, in some materials, as a specimen is stressed just past the point where it would otherwise exhibit an elastic response, it begins to strain harden and the forces required to continue into plastic deformation increase. If, at some arbitrary point, the forces acting on the body become

intermittent or specifically, forces which produce stresses beyond the proportional limit, then naturally, it would be logical to gauge the strain incrementally. Because this is an instantaneous measurement equivalent to the sum of all intermittent measurements, the equation for strain can be expressed as Equation 1, and is known as true strain, ϵ [2].

$$\epsilon = \int_{\ell_0}^{\ell_f} \frac{d\ell}{\ell} \quad \text{Eq. (1)}$$

This leads to the relationship between engineering stress, σ_e , and true stress, σ_t . During tensile testing, if we assume that the material experiences plastic incompressibility, or that there is no change in volume during plastic deformation, then we can say that the net volume remains constant and we can express any reduction in terms of area, A , or length, ℓ , as follows [3].

$$\Delta V = \ell'_1 \ell'_2 \ell'_3 - \ell_1 \ell_2 \ell_3 = 0 \quad \text{Eq. (2)}$$

$$1 = \frac{\ell'_1 \ell'_2 \ell'_3}{\ell_1 \ell_2 \ell_3} \quad \text{Eq. (3)}$$

$$1 = \frac{A' \ell'_3}{A_o \ell_3} \quad \text{Eq. (4)}$$

$$A' = \frac{A_o \ell_3}{\ell'_3} \quad \text{Eq. (5)}$$

In terms of engineering strain, $A' = A_o(1 - \epsilon)$ Eq. (6)

In terms of true strain, $A' = A_o e^{-\epsilon}$ Eq. (7)

From this, we recognize that true stress is not necessarily respective a specimens original unstressed area, but rather, respective of the specimens current stressed area (which may coincidentally be its original area). This can be expressed simply as:

$$\sigma_t = \frac{P}{A'} \quad \text{Eq. (8)}$$

However, it is logical to substitute for A_o , because A' to this point is unknown, and this equation becomes:

$$\sigma_t = \frac{P}{A_o} e^\epsilon \quad \text{Eq. (9)}$$

Furthermore, we know that engineering stress is calculated as,

$$\sigma_e = \frac{P}{A_o} \quad \text{Eq. (10)}$$

So, then the relationship between engineering and true stress becomes,

$$\sigma_t = \sigma_e e^\epsilon \quad \text{Eq. (11)}$$

Application of these concepts plays a vital role in failure analysis and ultimately failure prevention. Concepts of stress and strain will be used to analyze failure by fatigue and thermal boundary conditions. Additionally, during discussions of material selection in Appendix A, load case analysis in Appendix B and mechanical testing in Appendix C, we rely on our understanding of stress and strain to adequately assess results from theoretical and experimental calculations and tests.

2.2 Failure and Fatigue

2.2.1 Mechanical Fatigue

Understanding all the failure modes associated with the design of a structurally acceptable trailer goes beyond a simple static force analysis. Road going trailers undergo acceleration in the vertical, lateral, fore and aft directions, sometimes in excess of three times the acceleration of gravity. For heavy duty applications, these accelerations can lead to huge variations between static and dynamically applied loads. Additionally, random acceleration due to road surface variations and imperfections must be taken into consideration as these incident

loads will fatigue the materials in the structure and it has been accepted that metals subjected to these repetitive loads will exhibit lower resistance to failure than the same metal subjected to the same load in a static application.

An additional concern is failure under a static load case; however, in both cases, crack formation and propagation need to be at least minimally understood to properly evaluate a design. To deal with these possible modes of failure, we look at the most probable scenarios of brittle cracking and calculate a fracture toughness, K , based on common situations. Designs should be evaluated based on these potential failure modes and if the probable cause of failure cannot be easily determined, it may be reasonable to evaluate a change in design so that the failure modes can be factored more readily and more importantly, more accurately.

2.2.2 Methods for Analysis of Failure

Generalizing crack propagation and life cycles to failure can be difficult to do pre-failure; however, with some assumptions and estimations regarding crack size, initiation site and general knowledge of failure in this manner, close approximations are possible. With respect to static fracture analysis, take the equation for crack stress intensity factor and assume that a micro-crack or material surface flaw exists,

$$K_I = Y\sigma\sqrt{\pi a} \quad \text{Eq. (12)}$$

For a given condition, we can solve for σ either by the method shown in the previous section, by finite element analysis or by methods shown in later sections. The geometric factor, Y , can be taken as either 1 (through thickness crack), 1.1 (surface crack) or 1.12 (edge crack) [4] and, a , the crack size, can be calculated if the fracture toughness of the material is known. The plane strain fracture toughness is defined as,

$$K_{IC} = Y\sigma_f\sqrt{\pi a} \quad \text{Eq. (13)}$$

Where, σ_f is the stress at fracture. The fracture toughness of lower-strength steels can be difficult to deduce theoretically as these steels have a propensity for ductile crack extension prior to failure and therefore typical linear-elastic assumptions do not necessarily apply and elastic-plastic fracture mechanics methods must be utilized. These methods are outlined in ASTM E1820-18a, Standard Test Method for Measurement of Fracture Toughness, but require a pre-cracked specimen. If K_{IC} can be established, then imperfections can be evaluated as less than critical if, a , is satisfactorily less than the calculated result of [5],

$$a_{crit.} = \frac{K_{IC}^2}{\sigma^2 Y^2 \pi} \quad \text{Eq. (14)}$$

Additionally, the fatigue crack growth rate for a stress-intensity range can be expressed as [6],

$$\frac{da}{dN} = A\Delta K^m \quad \text{Eq. (15)}$$

Where, A and m are case specific constants and N is the number of cycles. Considering Equation 13, it follows that we can state ΔK^m as [6],

$$\Delta K^m = Y^m \sigma^m \pi^{m/2} a^{m/2} \quad \text{Eq. (16)}$$

Where ΔK^m is dependent on a change in either crack size or stress. With substitution and rearrangement, we can relate all these terms to the integrals of the change of crack size and number of cycles to failure [6],

$$\frac{1}{AY^m \sigma^m \pi^{m/2}} \int_{a_0}^{a_f} \frac{da}{a^{m/2}} = \int_0^{N_f} dN \quad \text{Eq. (17)}$$

Solving this expression and with the restriction of $m \neq 2$ yields,

$$N_f = \frac{a_f^{-(m/2)+1} - a_0^{-(m/2)+1}}{AY^m \sigma^m \pi^{m/2} [-(m/2) + 1]} \quad \text{Eq. (18)}$$

This is only valid over small growth increments and a_f must be first determined [6]. It is important to note that all fatigue calculations are temperature dependent. Also, of importance is the engineering strain rate $\left(\frac{d\varepsilon}{dt}\right)$, or rate of strain increase in a specimen over time. An example of how strain rate affects the fracture toughness is shown with respect to temperature in Figure 2.1.

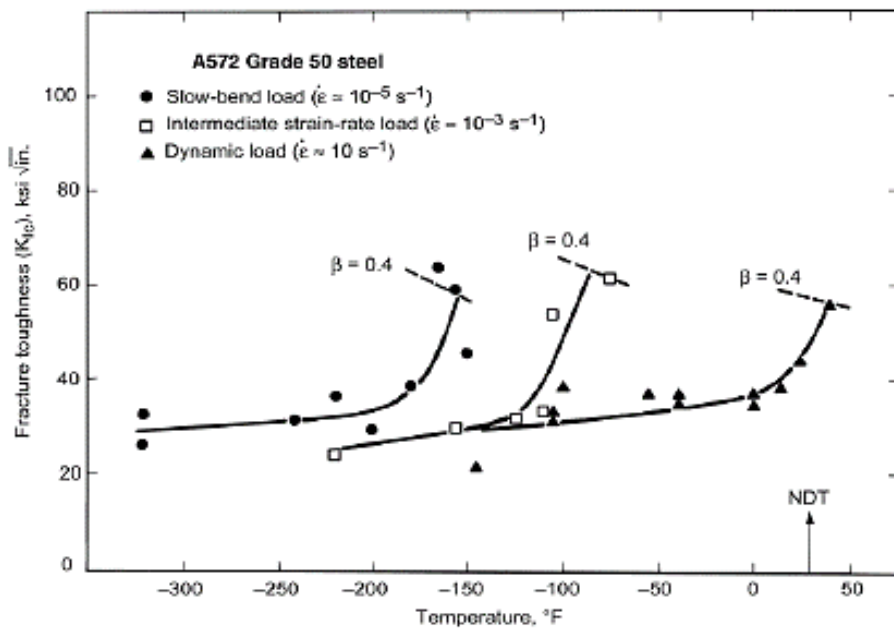


Figure 2.1 Effect of strain rate and temperature on fracture toughness [7]

A materials sensitivity to strain rate is roughly analogous to Holloman's equation where the working hardening coefficient, n , is replaced by a *strain-rate sensitivity index*, m : $\sigma = k'\dot{\varepsilon}^m$. Where, σ and k' are plastic stress and a strength coefficient and $\dot{\varepsilon} = \frac{d\varepsilon}{dt}$. In Holloman's equation these terms can be described by the curve of $\ln \sigma = n \ln \varepsilon + \ln k$. Note that $\ln k$ is the y-intercept of this curve [3].

2.2.3 Method for Estimating Fatigue Life

Fatigue life is often estimated based on strain range and additionally, the relationship between plastic strain range and elastic strain range which are related to the total strain by [8],

$$\Delta\varepsilon = \Delta\varepsilon_e + \Delta\varepsilon_p \quad \text{Eq. (19)}$$

where,

$$\frac{\Delta\varepsilon_e}{2} = \frac{\sigma'_f}{E} (2N_f)^b \quad \text{Eq. (20)}$$

and,

$$\frac{\Delta\varepsilon_p}{2} = \varepsilon'_f (2N_f)^c \quad \text{Eq. (21)}$$

Where, σ'_f and ε'_f are the fatigue strength and ductility coefficients and likewise, b and c are the fatigue strength and ductility exponents. The Method of Universal Slopes is a method outlined by S.S. Manson for approximating the strain range of a material at a given number of cycles and is provided as [8] [9],

$$\Delta\varepsilon = 3.5 \frac{UTS}{E} N_f^{-0.12} + \varepsilon_f^{0.6} N_f^{-0.6} \quad \text{Eq. (22)}$$

where,

$$\varepsilon_f = \ln\left(\frac{1}{1 - RA}\right) \quad \text{Eq. (23)}$$

and, RA is the reduction of area of a specimen at failure. Both the UTS and RA can be discovered via testing or taken from published tables. This method assumes that the elastic and plastic lines are the same for all materials³.

An extrapolation from the ASM Metals Handbook, shows that a numerical correlative estimate for non-austenitic steels can be made by relating the UTS and the hardness of the material as shown in Figure 2.2 Relationship between Rockwell hardness and UTS. It is

³ See page 963 in reference [9].

important to note that this correlation does not have a known metallurgical basis and should be used cautiously and only as a “ballpark” reference.

$$UTS = 12.751e^{0.0353R_A} \quad \text{Eq. (24)}$$

$$UTS = 15.638e^{0.0194R_B} \quad \text{Eq. (25)}$$

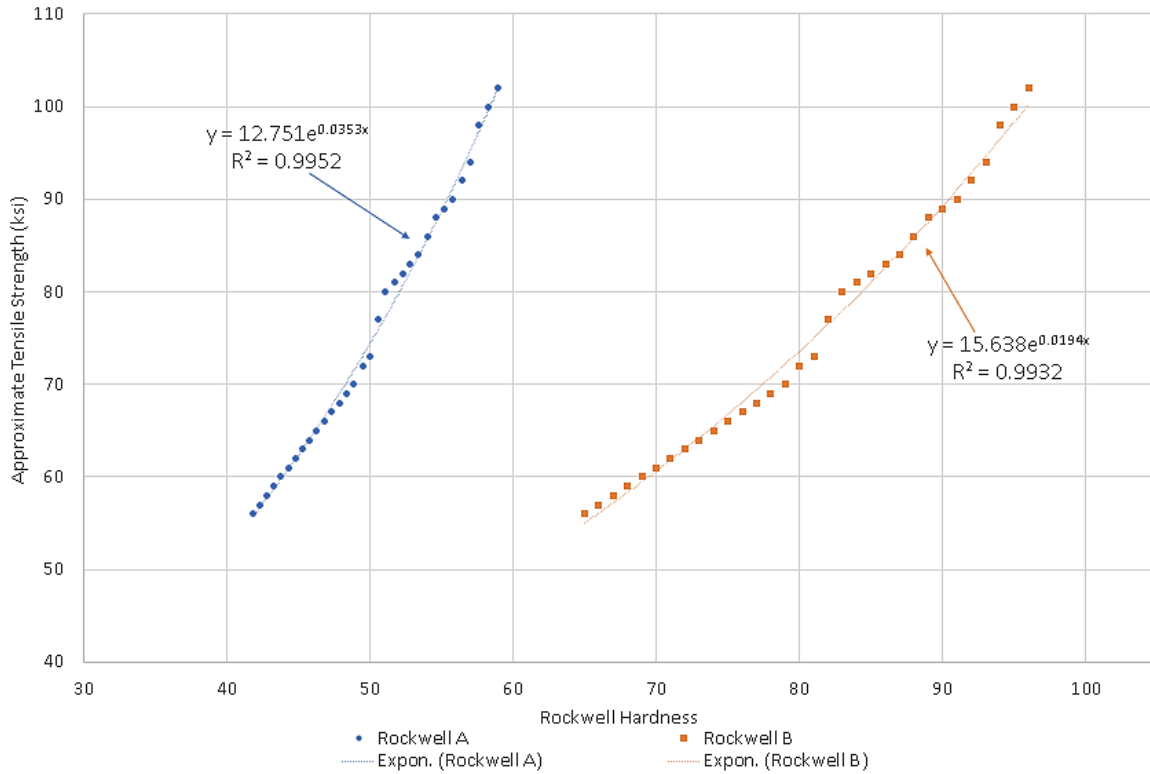


Figure 2.2 Relationship between Rockwell hardness and UTS

Perhaps a more approachable method is simple referencing of the applicable S-N curve. These curves, however, are not always readily available and it is therefore considered prudent to understand the concepts involving fatigue as presented in this work.

2.3 Welded Joint Design

2.3.1 Stress Analysis

For structural members, it is often mechanically- and more cost-effective to join materials via welding. In doing so, the added complications in a stress analysis must be considered. Special attention is required here because premature failures can occur even in joints fabricated in accordance with all applicable standards. This is partially due to the unavoidable additions of discontinuous geometry and partially due to changes in mechanical property of materials being joined with this process⁴.

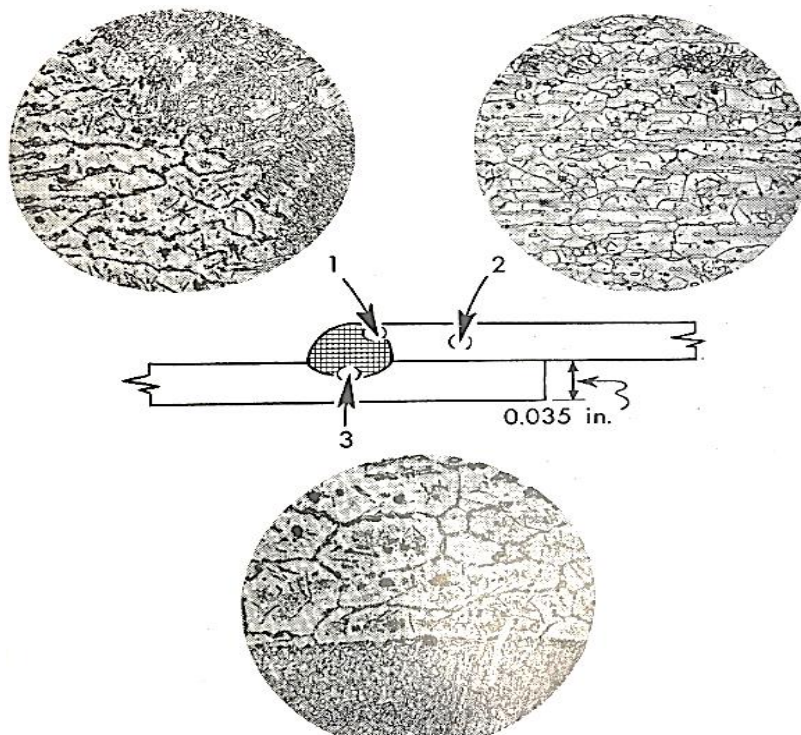


Figure 2.3 Representation of alteration in base material grain structure near a welded joint [10]

⁴ It should be noted that excessive welding should be avoided for these reasons.

The following figures and equations represent a general description of welded joints and how to analyze them.

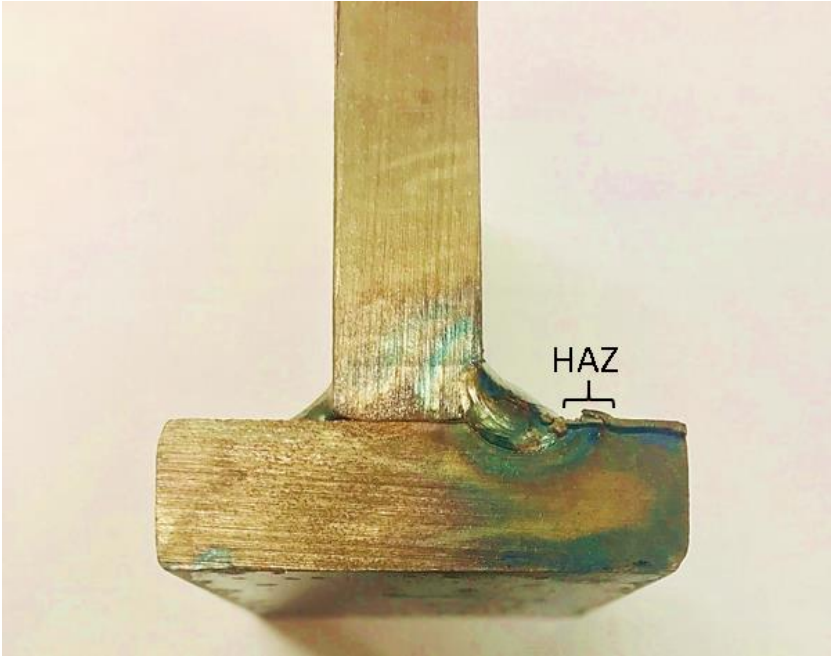


Figure 2.4 HAZ of a fillet weld

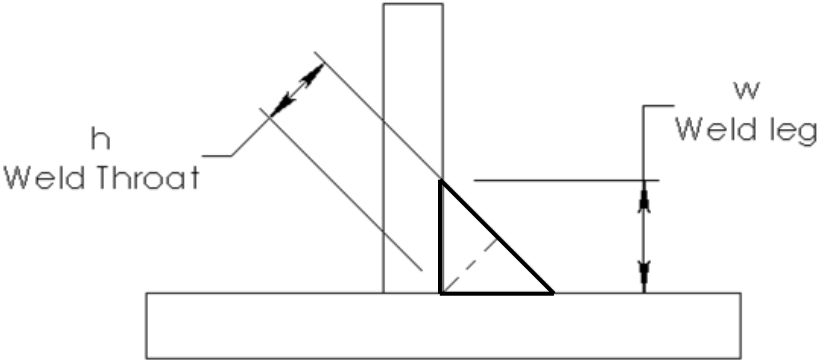


Figure 2.5 Reference figure for stress analysis showing weld parameters

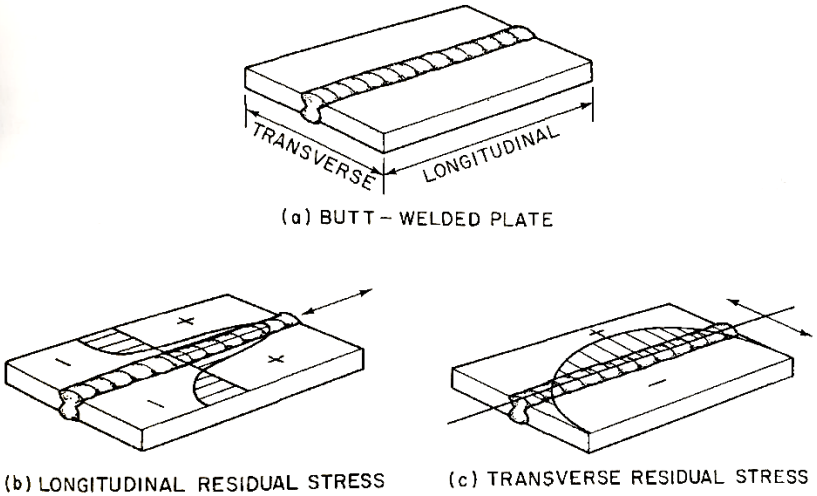


Figure 2.6 Reference directions for welded joints [7]

Tensile or Compressive Load Case

The following equation is valid for butt, V-groove or fillet welds [11]:

$$\sigma = \frac{F}{hL} \quad \text{Eq. (26)}$$

Where, σ is the average normal stress and L is the length of the weld.

Shear Load Case

The following equation is valid for butt, V-groove or fillet welds when the normal shear force passes through the weld centroid, and does not produce torsion [11]:

$$\tau = \frac{\text{Force}}{\text{Weld Throat Area}} = \frac{F}{wl\cos\varphi} \quad \text{Eq. (27)}$$

Where, φ is the angle of the leg, l . While it is desirable that $\varphi = 45^\circ$, it is not required. In the event that $\varphi \neq 45^\circ$, we must properly assess the joint stress and evaluate these equations as necessary.

Allowable Stress

The allowable stress in a weld can be calculated with the following formula [12].

$$F_V = 0.3F_{EXX}(1.0 + 0.5 \sin^{1.5} \Phi) \quad \text{Eq. (28)}$$

Where, F_{EXX} is the tensile strength of the electrode or weld wire and Φ is the angle of loading measured off the parallel axis of the weld. The minimum weld leg, w , can then be calculated using [13],

$$F = F_V A_W \quad \text{Eq. (29)}$$

Where,

$$A_W = N[wl\cos(\varphi)] \quad \text{Eq. (30)}$$

Where, N is the number of welds in the linear plane.

Fillet Weld Strength

Alternatively, for a fillet weld loaded longitudinally, the strength of the weld can be directly calculated as [14]:

$$R_n = 0.6F_{EXX} \frac{\sqrt{2}}{2} \frac{D}{16} L \quad \text{Eq. (31)}$$

Where, D is the size of the weld in 16th's of an inch.

2.3.2 Weldability

Welding involves changing the mechanical properties of steel by energy addition and control of cooling rates. As such, methods have been developed to analyze the thermal requirements of the joint to prevent cold cracking of the steel on cooling. In many cases, the temperature produced from the welding process alone is enough to maintain adequate cooling rates. In other cases, pre-heating or post-heating of the joint is required. Pre-heating lessens the

cooling rate of the joint, which allows for the material to maintain its ductility and it helps reduces the shrinkage or warpage in the joint. Additionally, by slowing the rate of cooling, trapped hydrogen is allowed more time to diffuse from the steel [15]. Determining the weld requirements starts with determining carbon equivalent of the base material.

The carbon equivalent (CE) is determined with the following formulae and application code [15] [16]. The maximum CE value for structural steel shapes with flanges less than 2 inch is 0.45% [17].

$$\text{Dearden-O'Neal} \quad CE = C + \frac{Mn}{6} + \frac{Cr + V}{5} + \frac{Ni + Cu}{15} \quad \text{Eq. (32)}$$

[16]

$$\text{American Welding Society}^5 \quad CE = C + \frac{Mn + Si}{6} + \frac{Cr + V + Mo}{5} + \frac{Ni + Cu}{15} \quad \text{Eq. (33)}$$

[15]

$$\text{Linnert [18]} \quad CE = C + \frac{Mn}{6} + \frac{Ni}{20} + \frac{Cr}{10} + \frac{Cu}{40} + \frac{Mo}{50} - \frac{V}{10} \quad \text{Eq. (34)}$$

Additionally, for high strength-low alloy steels [19],

$$CE = C + \frac{V}{10} + \frac{Mo}{15} + \frac{Cr}{10} + \frac{Mn + Cu + Cr}{20} + \frac{Si}{30} + \frac{Ni}{60} \quad \text{Eq. (35)}$$

At higher carbon levels, a non-linear correlation has been made [19]:

$$CE = C + A(C) \left(\frac{Cr + Mo + V + Nb}{5} + \frac{Mn}{6} + \frac{Cu}{15} + \frac{Ni}{20} \right) \quad \text{Eq. (36)}$$

Where,

$$A(C) = 0.75 + 0.25 \tanh[20(C - 0.12)] \quad \text{Eq. (37)}$$

⁵ This equation is also referenced by ASTM A992/A992M, Standard Specification for Structural Steel Shapes.

2.3.3 Considerations for Pre-Heating and Base Material Selection

Based on the results from the selected carbon equivalency equation, use the following figure to determine the zone. Evaluation of the different zones is as follows.

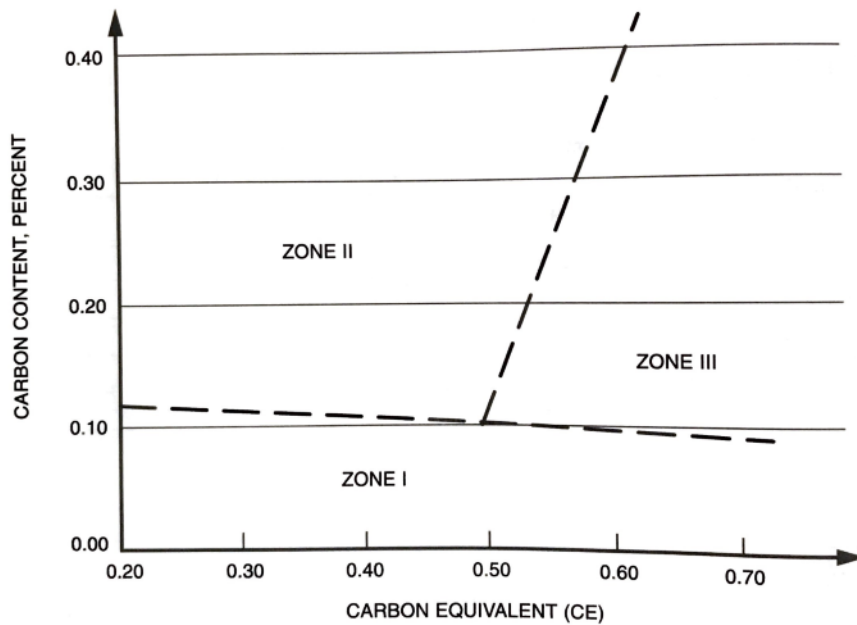


Figure 2.7 Zone classification of steels [15]

Zone I:

Cracking is unlikely, use low-hydrogen electrode if able and applicable and reference pre-heating tables as provided.

Zone II:

In this zone, the American Welding Society (AWS) recommends the hardness control method be used to determine the critical cooling rates required to prevent cracking. Irrespective of actual HAZ hardness, AWS recommends choosing a maximum hardness of either 350HV or

400HV. Then, Figure 2.8 can be used to determine the cooling rate at 540 °C. AWS D1.1 Annex H [15] provides additional tables, which can be used to select the actual cooling rate based on joint geometry, welding process and energy input. Figure is an example of one such table.

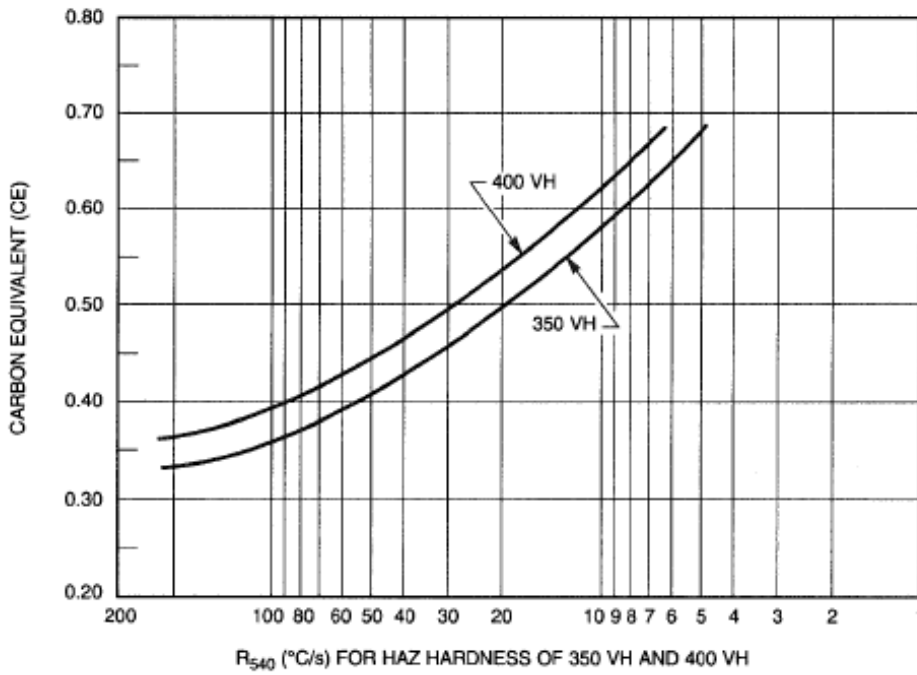


Figure 2.8 Critical Cooling Rates (CCR) based on CE [15]

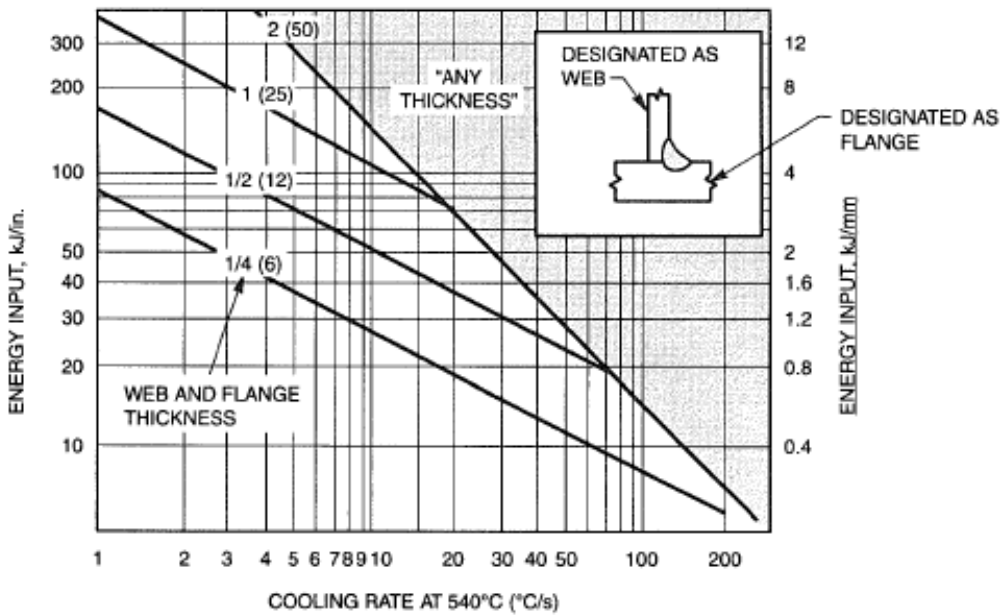


Figure 2.9 Cooling rate based on energy input and joint geometry [15]

Zone III:

In this zone, AWS recommends the hydrogen control method. Calculate the composition parameter, P_{cm}

$$P_{cm} = C + \frac{Ni}{60} + \frac{Si}{30} + \frac{Mn + Cu + Cr}{20} + \frac{Mo}{15} + \frac{V}{10} + 5B \quad \text{Eq. (38)}$$

Calculate the Susceptibility Index [15].

$$N = 12P_{cm} + \log_{10} H \quad \text{Eq. (39)}$$

Where, $H1 = 5$, $H2 = 10$ and $H3 = 30$. H is a reference to hydrogen or moisture levels in deposited weld material. $H1$ materials contain less than $5ml/100g$ of diffusible hydrogen content, $H2 < 10ml/100g$ and $H3$ materials are any materials not meeting the requirements of $H1$ or $H2$. Based on the value of N , categorize the result as A – G according to the following table.

Table 2.1 Susceptibility index rating

Susceptibility Parameter	Material Index
3.0	A
3.1 – 3.5	B
3.6 – 4.0	C
4.1 – 4.5	D
4.6 – 5.0	E
5.1 – 5.5	F
5.6 – 7.0	G

Match preheat temperature to values indicated on the following table.

Table 2.2 Minimum preheat and inter-pass temperatures °F [15]

Rigidity of Section	Thickness (in)	A	B	C	D	E	F	G
Low	<3/8	75	75	75	75	140	280	300
	3/8 - 3/4	75	75	75	140	210	280	300
	>3/4 - 1 1/2	75	75	75	175	230	280	300
	>1 1/2 - 3	75	75	100	200	250	280	300
	>3	75	75	100	200	250	280	300
Medium	<3/8	75	75	75	75	160	280	320
	3/8 - 3/4	75	75	75	175	240	290	320
	>3/4 - 1 1/2	75	75	165	230	280	300	320
	>1 1/2 - 3	75	175	230	265	300	300	320
	>3	200	250	280	300	320	320	320
High	<3/8	75	75	75	100	230	300	320
	3/8 - 3/4	75	75	150	220	280	320	320
	>3/4 - 1 1/2	75	185	240	280	300	320	320
	>1 1/2 - 3	240	265	300	300	320	320	320
	>3	240	265	300	300	320	320	320

With respect to critical cooling rates, ASM recommends the following formula to determine the cooling rate as allowable by the base material without increasing the risk of cracking [20].

$$CCR(^{\circ}F/s) = \frac{6.598}{CE - 0.3704} - 16.26 \quad \text{Eq. (40)}$$

2.4 Material Analysis

2.4.1 Material Selection

Material Shapes

Generally speaking, one can source a material in virtually any shape and size as some function of time, cost and mechanical property. Selection of material shape should be, at a high level, determined by functional requirements, load direction and magnitude, availability, feasibility and ancillary requirements such as finish or appearance. In terms of load case design constraints, one approach to material selection is a method of selection by required mass. In a general sense, we know that mass equals the product of area, depth and density and we can use this knowledge in combination with an understanding of the load case to determine the minimum requirements of the shape.

If we consider a simply supported beam, we can determine the required geometry based on mechanical properties and potential customer requirements. For example, one could use a W shaped beam (doubly symmetric wide-flanged I-Beam) fabricated from A572 Grade 50 and use a minimum design factor of safety of 1.67 and thus, the maximum allowable stress is 29,941 psi; which is practical only for static load cases. For dynamic loads, a factor of safety of at least 4.67 is recommended. This value comes from experimental data showing accelerations on average of

three times the standard acceleration of gravity during testing. Additionally, the customer could require that the design must meet certain dimensional requirements. Using the case of a simply supported beam which is supported at either end and has a resolved load in a variable location, we know that the maximum stress can be expressed as,

$$\sigma_{max} = \frac{-Pab}{Z\ell} \quad \text{Eq. (41)}$$

Where, a and b specify the location of the load, P , with respect to support locations, ℓ is the beam length and Z is the beam section modulus. In this equation, only the section modulus is unknown, and we can therefore rearrange to solve for this parameter. Knowing that the section modulus is the quotient of the second area moment of inertia and the beam centroid, we can further rearrange the equation to be represented by the constituents of the section modulus⁶.

$$\left[\frac{f_w(w_h + 2f_t)^3}{12} - \frac{(f_w - w_t)w_h^3}{12} \right] c^{-1} = \frac{-Pab}{\ell\sigma_{max}} \quad \text{Eq. (42)}$$

Where, f and w are flange and web and the subscripts w , h and t are width, height and thickness, respectively. From this, we can narrow down a list of W-beams which would meet the design criteria. From this list, considerations for cost and availability can be made to pick the most efficient beam. If mass is a design criterion, as is often the case, we can figure the feasibility of our selection based a calculation of the area.

$$A = 2(f_t f_w) + (w_h w_t) + \frac{\pi w_r^2}{4} \quad \text{Eq. (43)}$$

Recalling our definition of mass, we can very easily now make exclusions from our selections,

$$m = A\ell\rho \quad \text{Eq. (44)}$$

⁶ For the case of a doubly symmetric W-Beam. These calculations are shown in more depth in Appendix A

Real world applications are more complicated in that one must first figure the load case and then replicate the above method for torsion and compression considerations. From this we can conclude in agreement with the opening lines of this section; material selection is a function of design requirements, geometric variables and material properties [21].

2.4.2 Mechanical Properties, Behavior and Preferences

Brief Note on Metal Forming

Careful thought should be put into the selection of steel grades based on application. Materials to be machined or materials to be bent or otherwise cold-formed have additional requirements. For example, as a piece of sheet metal is being bent, the fibers along the outer radius will begin to experience tension and it follows that there is a measurable strain associated with this prescribed material elongation. The control feature is the inner radius of the bent part and the minimum of this radius has generally been defined as [22]:

$$r_{min} \equiv T \left(\frac{50}{r} - 1 \right) \quad \text{Eq. (45)}$$

Where, T is the material thickness and, r , is the percent reduction during tensile stressing of the material. Figure gives a generic representation of a v-bend operation. Often times bend radii are limited by the tools used and the capabilities of the bend operator.

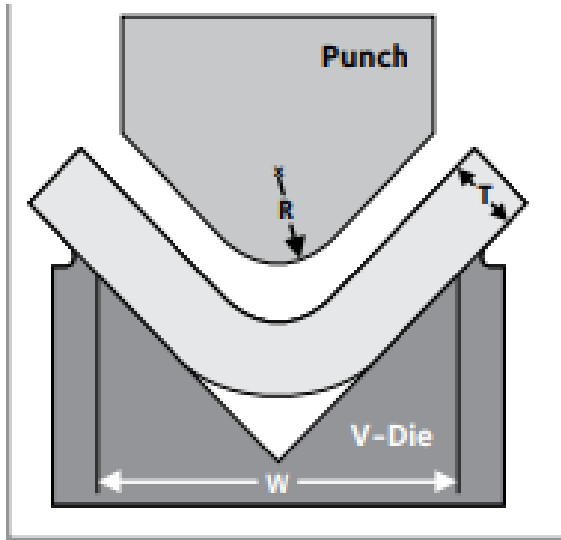


Figure 2.10 Typical forming visual description [23]

If we somewhat arbitrarily assign the published value for elongation percentage at break to r , we find that the resultant r_{min} may be satisfactory for a given application and as expected, will result in a value greater than the material thickness. If this method is chosen, it is recommended to use the elongation value related to the shortest specimen length and the resulting r_{min} value should be rounded to the nearest practical tool size. Alternatively, if we utilize Equation 6 and Equation 23, we can formulate r as follows:

$$r = 1 - e^{-\varepsilon_f} \quad \text{Eq. (46)}$$

However, more analytically, if we assume briefly that the strain is equal in the inner and outer fibers, we can express the strain in the outer fibers as [24],

$$\varepsilon = \frac{1}{(2r/T) + 1} \quad \text{Eq. (47)}$$

More to the point, if we describe ε as the strain at fracture in the outer radius we can rearrange this equation to represent r_{min} as [24],

$$r_{min} = \frac{T}{2} \left(\frac{1}{\varepsilon} - 1 \right) \quad \text{Eq. (48)}$$

Again, assigning the published values for percent elongation at break will produce satisfactorily conservative values for mild steels. Naturally, years of trial and error have drastically simplified this evaluation and the relationship between r_{min} and T is often simply stated as,

$$r_{min} = AT \quad \text{Eq. (49)}$$

Where, A is a constant which can be found by looking up an industry recommended value or adhering to a company standard. Generally, 1.5, 2 and 3 are acceptable values of A . For hot-dip galvanizing, the American Galvanizing Association recommends that $A=3$.

Material Preferences

There exist different preferences based on historic availability of suppliers and standards for plates, bars, tubing, pipe and structural members. The following tables from the AISC Steel Construction Manual illustrate these preferences.

Table 2-4 Applicable ASTM Specifications for Various Structural Shapes														
Steel Type	ASTM Designation	F _y Yield Stress ^a (ksi)	F _u Tensile Stress ^a (ksi)	Applicable Shape Series										
				W	M	S	HP	C	MC	L	HSS		Pipe	
											Rect.	Round		
Carbon	A36	36	58-80 ^b											
	A53 Gr B	35	60											
	A500	Gr. B	42	58										
			46	58										
		Gr. C	46	62										
	50		62											
	A501	Gr. A	36	58										
		Gr. B	50	70										
	A529 ^c	Gr. 50	50	65-100										
		Gr. 55	55	70-100										
	A709	36	36	58-80 ^b										
A1043 ^d	36	36-52	58											
	50	50-65	65											
High-Strength Low-Alloy	A572	Gr. 42	42	60										
		Gr. 50	50	65										
		Gr. 55	55	70										
		Gr. 60 ^e	60	75										
		Gr. 65 ^e	65	80										
	A618 ^f	Gr. Ia, Ib & II	50 ^g	70 ^g										
		Gr. III	50	65										
	A709	50	50	65										
		50S	50-65	65										
		50W	50	70										
	A913	50	50 ^h	65 ^h										
		60	60	75										
		65	65	80										
		70	70	90										
A992	50 ⁱ	65 ⁱ												
A588	50	70												
Corrosion Resistant High-Strength Low-Alloy	A847	50	70											

- = Preferred material specification.
- = Other applicable material specification, the availability of which should be confirmed prior to specification.
- = Material specification does not apply.

Figure 2.11 Preferential use of materials for structural shapes

Table 2-5														
Applicable ASTM Specifications for Plates and Bars														
Steel Type	ASTM Designation	F _y Yield Stress ^a (ksi)	F _u Tensile Stress ^a (ksi)	Plates and Bars, in.										
				to 0.75 incl.	over 0.75 to 1.25 incl.	over 1.25 to 1.5 incl.	over 1.5 to 2 incl.	over 2 to 2.5 incl.	over 2.5 to 4 incl.	over 4 to 5 incl.	over 5 to 6 incl.	over 6 to 8 incl.	over 8	
Carbon	A36	32	58-80											
		36	58-80											
	A283	Gr. C	30	55-75					d					
		Gr. D	33	60-80					d					
	A529	Gr. 50	50	70-100		b	b	b	b	b				
		Gr. 55	55	70-100		c	c	c	c	c				
A709	Gr. 36	36	58-80											
High-Strength Low-Alloy	A572	Gr. 42	42	60										
		Gr. 50	50	65										
		Gr. 55	55	70										
		Gr. 60	60	75										
		Gr. 65	65	80										
	A709	Gr. 50	50	65										
	A1043	Gr. 36	36-52	58										
Gr. 50		50-65	65											
Corrosion Resistant High-Strength Low-Alloy	A242	42	63											
		46	67											
		50	70											
	A588	42	63											
		46	67											
50	70													
Quenched and Tempered Alloy	A514	90	100-130											
		100	110-130											
Corrosion Resistant Quenched and Tempered Low-Alloy	A709	Gr. 50W	50	70										
		Gr. HPS 50W	50	70										
		Gr. HPS 70W	70	85-110										
		90	100-130											
		100	110-130											




 = Preferred material specification.
 = Other applicable material specification, the availability of which should be confirmed prior to specification.
 = Material specification does not apply.

Figure 2.12 Preferential use of materials for plates and bars

Tensile Requirements

While ASTM provides minimum tensile requirements as shown below for commonly used steels, these values can often lead to conservative designs. Using these values then provides an added measure of safety and as such is always acceptable for design practice.

Table 2.3 Tensile requirements of a few common steels [25] [26] [27]

Material	Minimum Yield Point (psi)	Minimum Tensile Strength (psi)
A500 Gr B	42,000	58,000
A36 Grade 36	36,000	58,000-80,000
A572 Grade 50	50,000	65,000

When purchasing steel, a certified MTR will display actual yield and tensile strengths tested in accordance with ASTM A6 and ASTM A370 as shown below. These values can be used to address safety factors for a specific application.

SPECIFICATIONS: Tested in accordance with ASTM specification A6/A6M-17a and A370, Quality Manual Rev H10 (3-14-19),
 AASHTO : M270-345M270-50-15
 ASME : SA-36 13
 ASTM : A992-11(13)/A36-14/A529-19-30/A572301811/A7093618/A7095018
 CSA : G40.21-44w/G40.2150WM

Description Part #	Heat# Grade(s) Test/Heat JW	Yield/ Tensile Ratio	Yield (PSI) (MPa)	Tensile (PSI) (MPa)	Elong %	C Cr XXXXXX	Mn Mo Tl	P Sb XXXXXX	S S XXXXXX	Si V N	Cu Nb XXXXXX	Ni CI XXXXXX	CE1 CE2 Pcm
W10x17 060' 00.00' W250X25.3 018.2880m B1017W14000720	2800323 A992-11(15)	.83	56700 391	68000 469	27.90	.07 .03	.83 .01	.008 .0035	.018 .0001	.20 .003 .0040	.07 .026	.03 2.15	.22 .2570 .1208 InvH: 1913133
W10x19 060' 00.00' W250X28.4 018.2880m B1019W14000720	2804027 A992-11(15)	.82	56200 387	68600 473	24.95	.07 .04	.82 .01	.010 .0045	.022 .0001	.20 .003 .0056	.08 .026	.03 2.41	.22 .2615 .1242 InvH: 1913133
W10x22 060' 00.00' W250X32.7 018.2880m B1022W14000720	2803768 A992-11(15)	.83	56600 390	68300 471	25.73	.07 .05	.89 .01	.016 .0056	.021 .0001	.21 .006 .0044	.10 .028	.03 3.05	.23 .2743 .1262 InvH: 1913133

Figure 2.13 Sample certified mill test report for A572 grade 50 steel W-shapes

Table 2.4 shows that on average, the as-received steel is of higher grade than the minimum grades as required by ASTM. This exemplifies the importance of receiving a mill test certificate for structural steels.

Table 2.4 Collected average values for common steels

Material	Yield (psi)	UTS (psi)	Susceptibility	Weldability
A36	50,416.00	71,221.50	0.355	0.338
A572 Gr 50	55,618.18	70,563.64	0.328	0.314

Chemical Limitations

Understanding the chemical makeup of the steels being utilized for construction is nearly as important as understanding their mechanical properties. While these values will be listed on an MTR as well, ASTM provides maximum values. Each element plays a role in the final steel qualities, albeit some roles are better understood than others. Carbon is the primary hardening element in steel; however, it has deleterious effects as a consequence such as producing a poor surface finish in some cases [20] and notably, reducing ductility and weldability as previously discussed. Chromium has a mostly singular function which is to increase the corrosion resistance of the steel. Niobium is added to increase the yield strength and to some degree, the tensile strength. Copper, like chromium, increases the corrosion resistance of the steel; however, like carbon it has a negative effect on surface finish. Manganese and phosphorus serve to increase the strength of the steel. Sulfur is only used to increase machinability, however, it negatively effects, notch toughness and surface finish. Silicon and aluminum are added to control grain size and aid in the reduction of oxygen formations. Nickel and boron are used to increase hardenability and molybdenum is used to decrease susceptibility to embrittlement [20].

Everything is better in moderation and the addition of these elements is no exception. ASTM standards limit the use of elements in certain steels to control quality and conformance. Table 2.5 lists the ASTM standard percentages of elements in three common steel grades.

Table 2.5 Chemical composition as a percentage of typical steels [25] [26] [27]

	Composition (in wt. %) of Different Steels		
	A1011 Grade 33	A36 Grade 36	A572 Grade 50
Carbon, C	0.250	0.260	0.230
Chromium, Cr	0.150	0.000	0.350
Niobium, Nb	0.000	0.000	0.050
Copper, Cu	0.200	0.200	0.600
Manganese, Mn	0.900	0.000	1.350
Molybendum, Mo	0.060	0.000	0.150
Nickel, Ni	0.200	0.000	0.000
Niobium, Nb	0.008	0.000	0.000
Phosphorous, P	0.035	0.004	0.030
Silicon, Si	0.000	0.004	0.400
Sulfur, S	0.040	0.005	0.030
Titanium, Ti	0.025	0.000	0.000
Vanadium, V	0.008	0.000	0.150

Realistically, these values are conservative and if it is required to know the chemistry of steel in use, a Mill Test Report (MTR) should be requested from the source.

2.5 Thermal Considerations

2.5.1 Topics on Galvanizing

Introduction to Galvanizing and Its Purpose in Industry

Galvanized coatings take advantage of the anode-cathode relationship between zinc and the steel base material. Because zinc has a greater propensity to go into a corrosive solution, such as the salty air as can be found in coastline environments, it will continuously “protect” the steel by sacrificing itself [28]. Additionally, zinc protects the base steel simply by preventing moisture from contacting the steel and therefore there exists no electrolyte to facilitate corrosion. Zinc coatings also continue to provide protection where there may be a small exposed area of the base

steel. There are, however, serious considerations to be taken into account when deciding to hot-dip galvanize a product as previously mentioned.

Given the reactive nature of steel contact with silicon, galvanizers have traditionally added other elements to aid in stabilizing the reaction. When choosing a supplier for galvanizing needs, it is worth noting the effects of these additives. Particularly, one should note the melting temperatures of additives and surface finish of the materials to be galvanized. If a surface includes cracks, voids or grain defects, the liquid metal (zinc plus additives) may enter the structure of the material and naturally, as the liquid constituents cool and freeze at rates unique to their thermomechanical properties, propagation of these defects can occur. This propagation may be caused by tensile stresses induced from the contraction of the cooling steel surrounding the liquid or solid pools of galvanizing elements and varying temperature gradients produced from the cooling of these unique elements.

The Japanese Industrial Standard G 3129 stipulates that the following formula be used to determine the crack equivalent of sensitivity of a particular steel to be hot-dip galvanized.

Results from this formula should be less than 45% (elements are percent mass of total) [1].

$$ES = C + \frac{Si}{17} + \frac{Mn}{7.5} + \frac{Cu}{13} + \frac{Ni}{17} + \frac{Cr}{4.5} + \frac{Mo}{3} + \frac{V}{1.5} + \frac{Nb}{2} + \frac{Ti}{4.5} + 420B \quad \text{Eq. (50)}$$

<u>Additive</u>	<u>Zone Affected</u>	<u>Primary Effect</u>
Al	Outer Zinc Layer	Adds “brightness” to initial coating appearance
Pb	Outer Zinc Layer	Historically found in some grades of zinc, significantly affects drainage by lowering surface tension
Ni	Intermetallics	Inhibits Silicon effect within certain ranges
Bi	Outer Zinc Layer	Has similar effect as Pb, reportedly also has reactivity effect when used with Sn
Sn	Both Zones	Inhibits silicon reaction within certain ranges, improves drainage of excess zinc as the outer layer forms, and can also enhance “spangled” and “brightness” appearance of outer layer

Figure 2.14 Effects of zinc additives to galvanized materials [29]

Regarding the elements listed in Figure 2.14, a study by Poag and Zervoudis [30]⁷ has shown that lead leads to increase failure occurrence, nickel had no significant effect on cracking and tin or bismuth concentrations in excess of 0.2% increased failure occurrence during the dipping process [29].

⁷ Study results as discussed in reference [25]

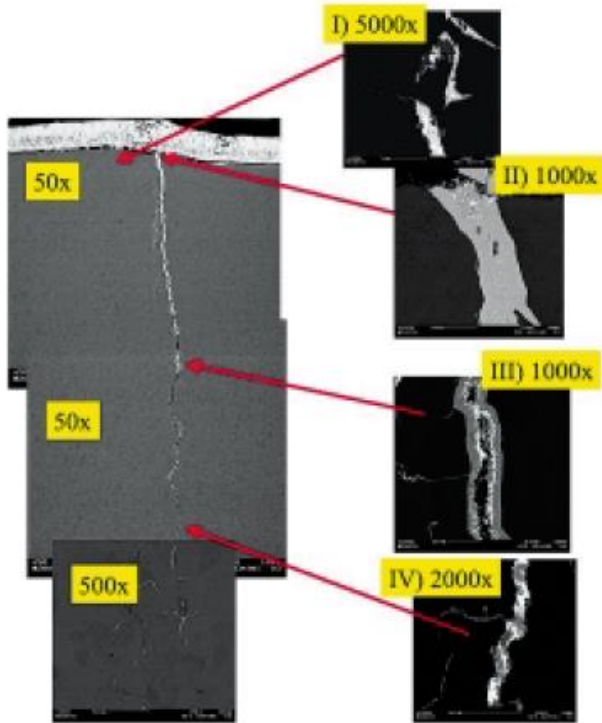


Figure 2.15 Micrograph of LMAC caused by infiltration of galvanizing bath constituents into the base material [1]

Brief Weight Gain Discussion

Because a zinc coating will continuously sacrifice itself to the environment, the effectiveness of the coating and the longevity of the coating can be related directly to the coating thickness [31]. As such, it is important to consider the additional weight added to any structure as this weight gain is related to the coating thickness and can add a significant load to the structure.

Table 2.6 Coating thickness and weight [32]

Coating Grade	Coating Thickness (mils)	Weight (oz/ft ²)
35	1.40	0.80
45	1.80	1.00
50	2.00	1.20
55	2.20	1.30
60	2.40	1.40
65	2.60	1.50
75	3.00	1.70
80	3.10	1.90
85	3.30	2.00
100	3.90	2.30

Table 2.6 shows the minimum coating thicknesses per ASTM 123A, but does not necessarily take the chemical composition of the steel into consideration. As such, a simple correlation is formed in this study which compares mil thickness to weight per surface area.

$$\chi = -0.0046\xi^2 + 0.6359\xi - 0.0914 \quad \text{Eq. (51)}^8$$

Where, ξ , is a mil thickness predicted in this study by an extrapolation of a typical Sandelin curve.

$$\begin{aligned} \xi = & 32469Si^6 - 28166Si^5 + 3313.1Si^4 + 3287.2Si^3 - 1135.4Si^2 \\ & + 115.09Si - 0.1092 \end{aligned} \quad \text{Eq. (52)}^9$$

Where, Si is the silicon content as a percentage by weight; for example, 0.28 for 0.28%. Kinstler suggests that a *silicon equivalent* be used to account for the effect of phosphorus [29].

$$Si(equiv) = Si\% + 2.5P\% \quad \text{Eq. (53)}$$

⁸ $R^2 = 0.9918$.

⁹ $R^2 = 0.97$. It should be noted that this formula becomes less accurate for Sandelin steels (0.06% - 0.13% Si).

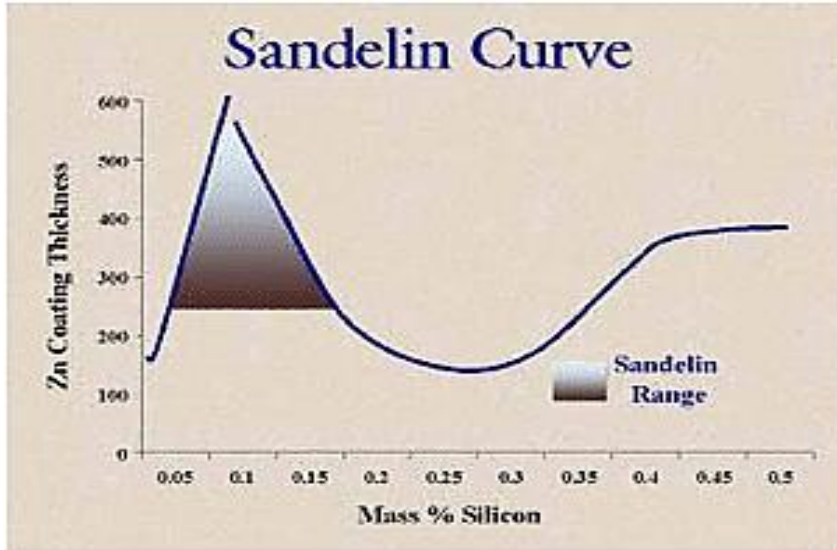


Figure 2.16 Typical Sandelin curve comparing coating thickness to mass percent silicon [33]

ASTM A385 [34] recommends steels for use with structures to be hot-dip galvanized should be limited to silicon ranges of $0.04\% > Si < 0.06\%$ and $0.15\% > Si < 0.22\%$ with an absolute maximum silicon content of 0.25%.

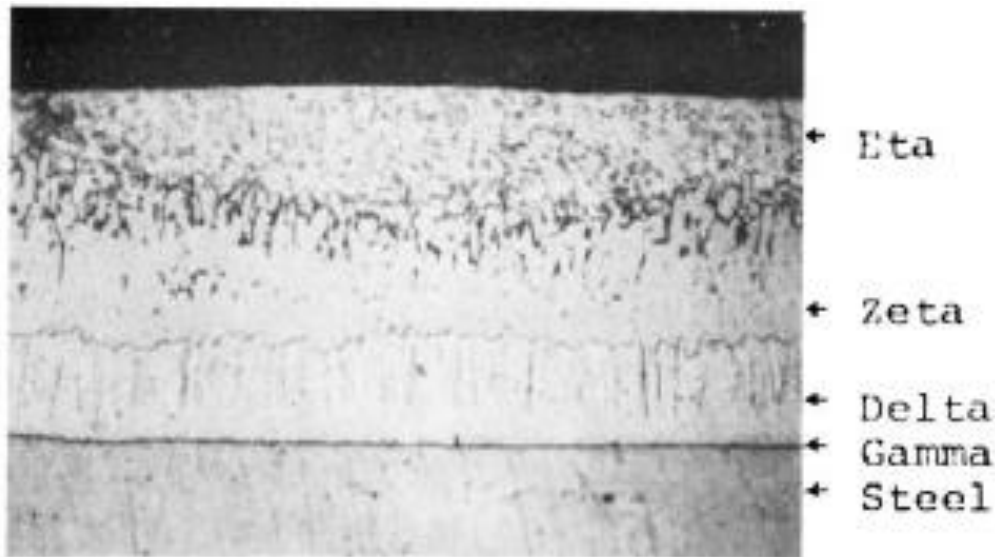


Figure 2.17 Galvanized coating on properly selected steel [34]

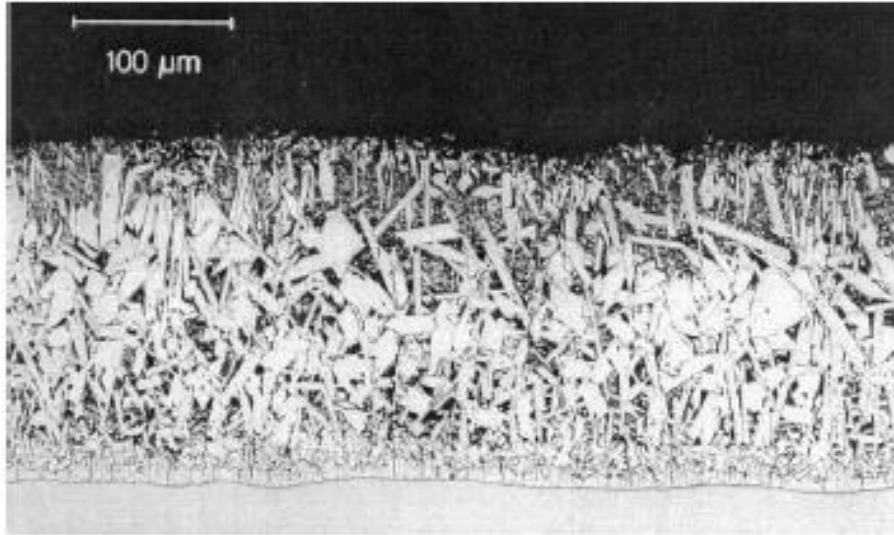


Figure 2.18 Galvanized coating on a Sandelin steel [34]

These calculations allow for corrections of thicker coatings than ASTM standards provide – which is often the case. The equation for estimated weight gain in pounds is then,

$$w = \frac{\mathbb{D}A_s\chi}{16} \quad \text{Eq. (54)}$$

Where, A_s , is the total surface area of the weldment being dipped in square feet and \mathbb{D} , is a design factor. Design considerations are: Silicon content in the steel, proper drainage for hollow sections, edge geometry and weldment size. A good starting value for \mathbb{D} is 2; however, \mathbb{D} can vary significantly. A suggested range to consider would be: $1 \leq \mathbb{D} \leq 2.5$. Good communication with the galvanizer can help determine an accurate value for \mathbb{D} .

Discussion on Hydrogen Embrittlement

Irrespective of temperature, hydrogen, when exposed to raw steel, will diffuse through the material. Because of its relative elemental size, hydrogen can theoretically move freely through the steels lattice. Research and experimental testing by Grabke and Reicke and Kim et.

al., indicate that not only do hydrogen diffusion rates increase with temperature but also by tensile stressing of the material. Additionally, their research seems to confirm the hypothesis of hydrogen trapping [35] [36]. As absorbed hydrogen diffuses through the steel, it can become concentrated in these trapping sites as well as any other defects in the material and generate internal pressure. The hydrogen can also therefore disrupt the lattice structure. A combination of these effects can assist in material cracking and significantly reduce a materials strength.

Hydrogen tends to allocate itself in areas of high hydrostatic tensions. Therefore, in areas of non-uniform hydrostatic stress, such as the heat affected zones near a welded joint, there exists a higher propensity for hydrogen collection. This localized concentration of hydrogen can be described by [37],

$$\ln\left(\frac{C_H}{C_0}\right) = \frac{\Omega\sigma_P}{RT} \quad \text{Eq. (55)}$$

Where, C_H and C_0 are the hydrogen and local equilibrium concentrations and Ω and σ_P are the molar volume of hydrogen and hydrostatic stress, respectively.

This diffusion can occur during oxidization in a case where the reaction results in a hydrogen ion, exposure to fresh water and especially in salt water environments where many of the chemical constituents in the water contain some form of a hydrogen ion. Additionally, contact with cleaning (pickling) solutions of sulfuric (H_2SO_4) and hydrochloric (HCL) acids can result in elevated hydrogen diffusion [28]. Generally speaking, the effects of hydrogen in steel are fairly well documented, however, there has yet to be developed a clear numerical method to predict the mechanisms of failure. As such, care should be taken to minimize hydrogen exposure – especially at elevated temperatures.

2.6 Discussion of Material Properties at Elevated Temperatures

2.6.1 Steel at Elevated Temperatures

Mechanical Properties of Steel at Elevated Temperatures

Areas where thermal effects are of highest interest are hot-dip galvanizing and welding. The influence of temperature on steel has long been studied and several sources have found, or otherwise derived mathematical expressions which describe the relationships between mechanical properties and temperature. Naturally, it can be an arduous endeavor to resolve, by hand, the boundary conditions for a large complex welded structure of varying material property into usable information; however, to make decisions with good judgement, it is necessary to understand the boundary conditions and their role in the analysis of structures.

While the American Institute for Steel Construction provides values specific to steels less than 65ksi in yield strength (see Figure 2.21 Exact values of steel strength at elevated temperatures), the following calculations are based on the AISC's Specification for the Design, Fabrication, and Erection of Structural Steel for Buildings and ASTM E119, Standard Test Methods for Fire Test of Building Construction and Materials. For temperatures between and including zero and 600°C [38],

$$\sigma_{yT} = \left[1 + \frac{T}{900 \ln(T/1750)} \right] \sigma_y \quad \text{Eq. (56)}^{10}$$

$$E_T = \left[1 + \frac{T}{2000 \ln(T/1100)} \right] E \quad \text{Eq. (57)}$$

¹⁰ According to the European Convention for Constructional Steelwork, this equation uses the constant 767 instead of 900.

Where, σ_{yT} and E_T are the yield strength and modulus of elasticity at temperature, respectively and σ_y and E are the same parameters for published values at 20°C (68°F). For temperatures up to 650°C (1200°F), the linear coefficient of thermal expansion can be expressed as [39]:

$$\alpha_T = (11 + 0.0062T) \times 10^{-6} \quad \text{Eq. (58)}$$

For temperatures greater than 600°C [38],

$$\sigma_{yT} = \frac{340 - 0.34T}{T - 240} \sigma_y \quad \text{Eq. (59)}$$

$$E_T = \frac{690 - 0.69T}{T - 53.5} E \quad \text{Eq. (60)}$$

$$\alpha_T = (0.004T + 12) \times 10^{-6} \quad \text{Eq. (61)}$$

From these results, the stress strain relationships are developed for our materials [39].

Firstly, it is noted the difference between the strain related to the proportional stress-strain relationship, ε_p and the actual strain experience by the steel, ε_s .

$$\varepsilon_p = \frac{0.975\sigma_{yT} - 12.5\sigma_{yT}^2}{E_T - 12.5\sigma_{yT}} \quad \text{Eq. (62)}$$

For the case of $\varepsilon_s \leq \varepsilon_p$,

$$f_T = E_T \varepsilon_s \quad \text{Eq. (63)}$$

Where, f_T is the strength of the steel. For the case of $\varepsilon_s > \varepsilon_p$,

$$f_T = (12.5\varepsilon_s + 0.975)\sigma_{yT} - \frac{12.5\sigma_{yT}^2}{E_T} \quad \text{Eq. (64)}$$

An alternate and more conservative method according to Lie and Stanzak [40] [39] is:

$$\sigma_{yT} = \sigma_y(1 - 0.78\theta - 1.89\theta^4) \quad \text{Eq. (65)}$$

$$E_T = E(1 - 2.48\theta^2) \quad \text{Eq. (66)}$$

Where,

$$\theta = \frac{T - 68}{1800} \quad \text{Eq. (67)}$$

Another method is presented by the National Institute of Standards and Technology [41] and attempts to predict the Young's modulus and Poisson's ratio as functions of temperature. E is given in GPa and T in Celsius.

$$E_T = E + e_1T + e_2T^2 + e_3T^3 \quad \text{Eq. (68)}$$

Where,

$$e_1 = -0.04326$$

$$e_2 = -3.502 \times 10^{-5}$$

$$e_3 = -6.592 \times 10^{-8}$$

$$\nu_T = \nu + \nu_1T + \nu_2T^2 + \nu_3T^3 + \nu_4T^4 \quad \text{Eq. (69)}$$

Where,

$$\nu_1 = 2.5302417 \times 10^{-5}$$

$$\nu_2 = 2.6333384 \times 10^{-8}$$

$$\nu_3 = -9.9419588 \times 10^{-11}$$

$$\nu_4 = 1.2617779 \times 10^{-13}$$

These methods can be used to predict the maximum allowable¹¹ strain by using Hooke's Law¹²:

$$\varepsilon = \frac{\sigma_y}{E} \quad \text{Eq. (70)}$$

¹¹ Strain which falls on the stress-strain curve prior to the proportional limit and the non-linear stress-strain relationship thereafter.

¹² This assumption should be verified by first article inspection.

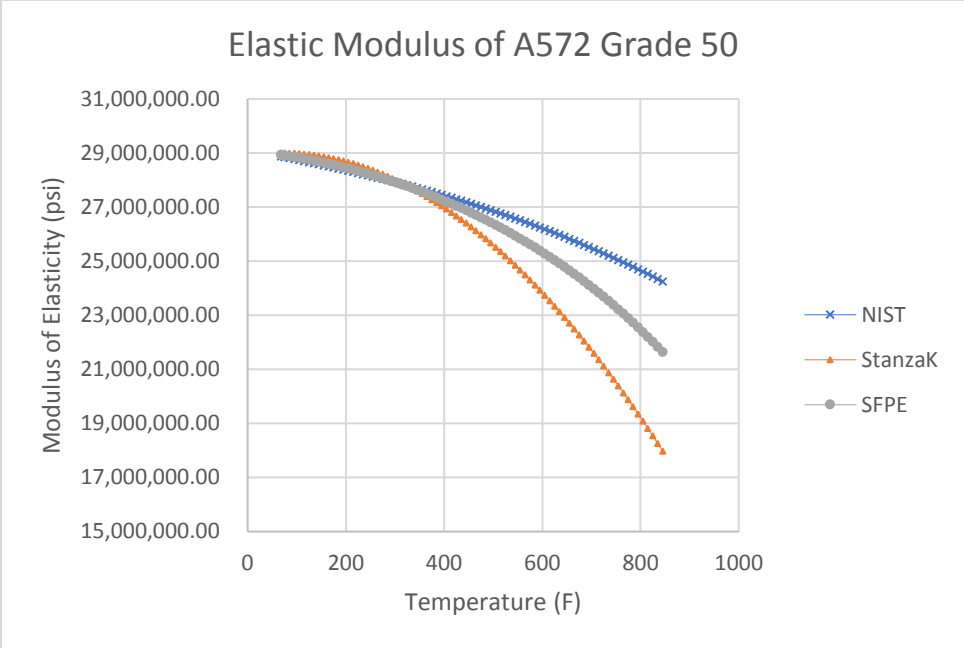


Figure 2.19 Comparison of methods for calculating the elastic modulus verse temperature

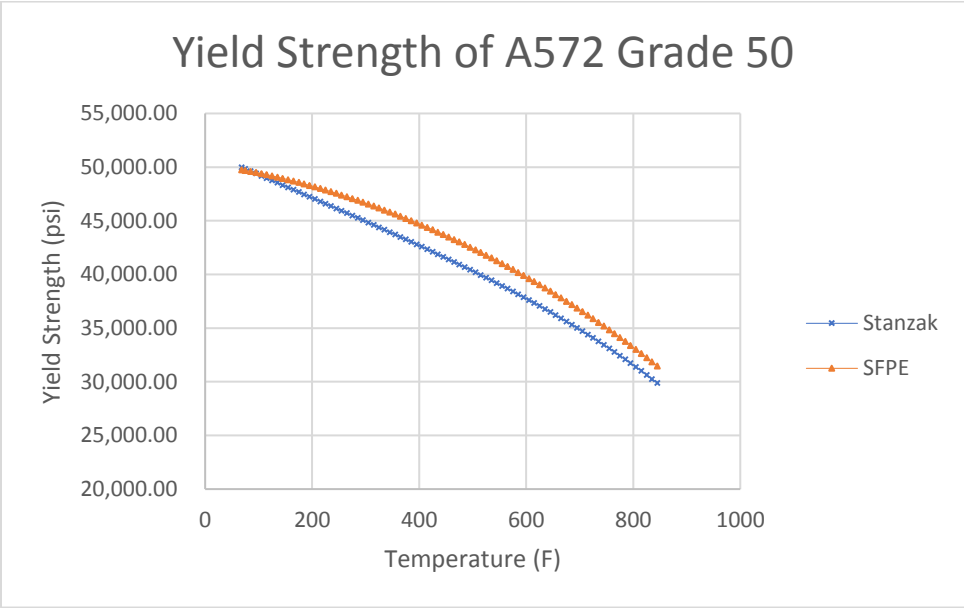


Figure 2.20 Comparison of methods for calculating the yield strength verse temperature

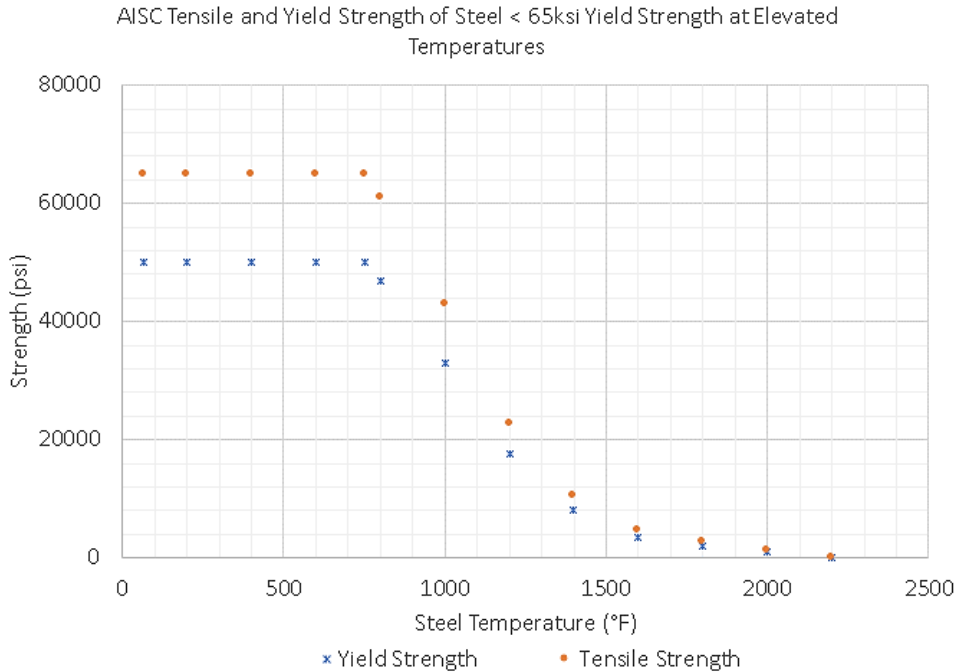


Figure 2.21 Exact values of steel strength at elevated temperatures [38]

Thermophysical Properties of Steel at Elevated Temperatures

Given the previous discussion on the mechanical properties of steel at elevated temperatures, it is easily understood that the thermophysical properties change as well. Calculate the thermal diffusivity:

$$\alpha = \frac{k}{c_p \rho} \tag{Eq. (71)}$$

Where, k , c_p , and ρ are thermal conductivity, specific heat capacity and density, respectively.

While, it may be that thermal conductivity is dependent on the chemical constituents of steel at room temperature, at elevated temperatures, k can be described as non-variant amongst steel and can be calculated with the following equation. [39].

$$k = -2.9436 \times 10^{-7}(T - 2181.82) \text{ for } 0 \leq T \leq 900^{\circ}\text{C} \quad \text{Eq. (72)}^{13}$$

The product of specific heat capacity and density can be considered as the volumetric heat capacity of a material. This relationship is useful in calculating the thermal diffusivity of a material and can be calculated by [39]¹⁴:

$$\rho c_p = 0.000062(T + 825) \quad \text{Eq. (73)}^{15}$$

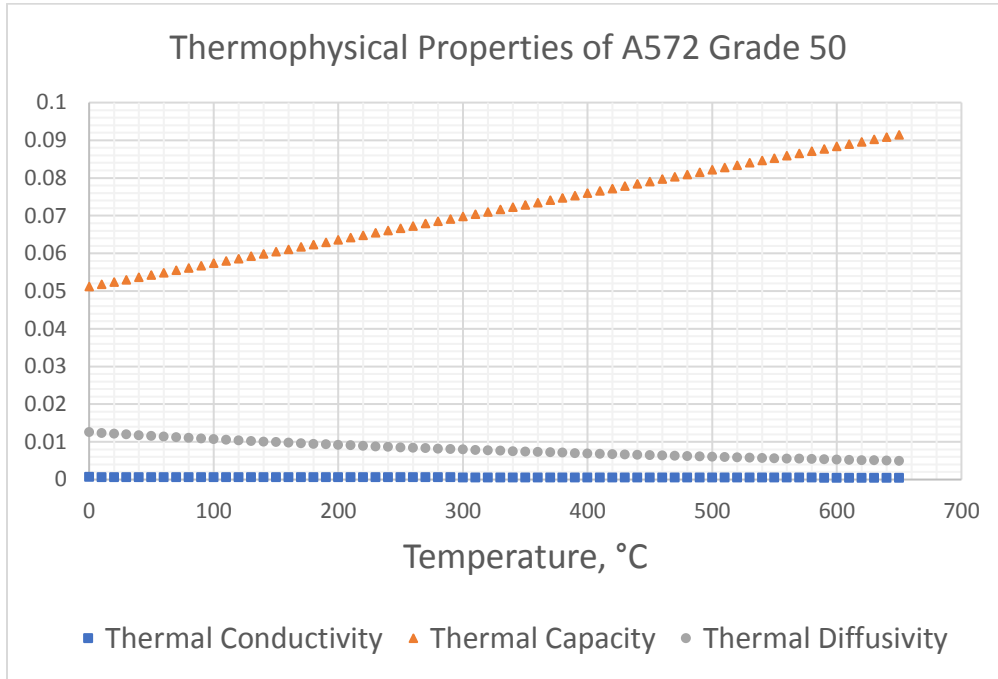


Figure 2.22 Theoretical thermophysical properties of A572 grade 50

¹³ The original equation can be found on page 17 of the referenced text. The equation presented in this thesis is adapted for the units ($BTU/sec \cdot in \cdot ^{\circ}C$).

¹⁴ For $0 \leq T \leq 650^{\circ}C$

¹⁵ The original equation can be found on page 222 of the referenced text. The equation presented in this thesis is adapted for the units ($Btu/in^3 \cdot ^{\circ}C$).

2.6.2 Zinc at Elevated Temperatures

Thermophysical Properties of Zinc at Elevated Temperatures

Given that the zinc in this case is liquid and that it is unlikely to be pure zinc, certain assumptions and calculations must be made to predict the thermophysical material properties. Based on a linear regression analysis showing acceptable uncertainties, the density of liquid zinc meeting the restrictions shown in the following figure can be calculated as follows [43].

$$\rho = c_1 - c_2(T - T_{ref}) \quad \text{Eq. (74)}$$

	T_{range} (K)	c_1 (kg m ⁻³)	c_2 (kg m ⁻³ K ⁻¹)	T_{ref} (K)	Deviation (2 σ) (%)
Cadmium	594–833	8008	1.251	594.219 (Ref. 71)	0.6
Cobalt	1768–2500	7827	0.936	1768.0 (Ref. 72)	2.1
Gallium	303–1500	6077	0.611	302.914 (Ref. 73)	0.4
Indium	430–1100	7022	0.762	429.748 (Ref. 73)	0.5
Silicon	1687–2000	2550	0.264	1687.0 (Ref. 41)	2.2
Thallium	576–1200	11233	1.200	576.7 (Ref. 74)	0.9
Zinc	692–910	6559	0.884	692.677 (Ref. 73)	0.7

Figure 2.23 Coefficients for density calculation

The values produced from this calculation can be verified by published data respective to zinc at various temperatures [44].

For the purpose of calculating a convection coefficient, we must first find the kinetic viscosity of zinc at the tank temperature and because the density varies only with temperature at constant pressure, we can calculate the fluid volumetric expansion coefficient.

$$\nu = \frac{\mu}{\rho} \quad \text{Eq. (75)}$$

Where, μ is the dynamic viscosity¹⁶. The viscosity can alternatively be calculated as [45]¹⁷:

$$\eta = \eta_0 \exp\left(\frac{E}{RT}\right) \quad \text{Eq. (76)}^{18}$$

Where, η_0 ($mNsm^{-2}$) and E ($J \cdot K^{-1}mol^{-1}$) are constants and for elevated temperatures in the realm of galvanizing can be considered as, 0.4131 and 12.7 respectively. R is the gas constant ($8.3144J \cdot K^{-1}mol^{-1}$).

Utilizing the Stokes-Einstein Theory, the diffusivity constant can then be approximated by [45]:

$$D = \frac{\kappa_B T}{6\pi R\eta} \quad \text{Eq. (77)}$$

Where, κ_B is the Boltzmann constant¹⁹. This is relevant if the diffusivity constant of the steel is known and if a deeper understanding of the zinc coating is desired. The fluid property of volumetric expansion is expressed as [46],

$$\beta = -\frac{1}{\rho} \left(\frac{\partial \rho}{\partial T}\right)_p \quad \text{Eq. (78)}$$

This can be expressed approximately as:

$$\beta \approx -\frac{1}{\rho} \frac{\Delta \rho}{\Delta T} = -\frac{1}{\rho} \frac{\rho_\infty - \rho}{T_\infty - T} \quad \text{Eq. (79)}$$

¹⁶ These values have been interpolated successfully from Assael Et Al. for elevated temperatures.

¹⁷ While not necessarily applicable to this particular case, the following relationship between surface tension and viscosity can be employed: $\gamma = \eta \frac{15}{16} \sqrt{\frac{\kappa_B T}{m}}$, where, m is the atomic mass.

¹⁸ Units of $mNsm^{-2}$. mN can be converted to *kilogram – force* by multiplying by 4.222×10^{-5} , yielding $kgf \cdot s \cdot m^{-2}$.

¹⁹ $\kappa_B = 1.3806 \times 10^{-23} m^2 \cdot kg \cdot s^{-2} \cdot K^{-1}$.

If published data is not available, the specific heat capacity and thermal conductivity of pure zinc at an elevated temperature can be estimated respectively, by the following extrapolations [45] [47],

$$c_p = -T^3 10^{-6} + 0.0011T^2 - 0.12T + 404 \quad \text{Eq. (80)}^{20}$$

$$k = -2T^3 10^{-7} + 0.0001T^2 - 0.0583T + 114 \quad \text{Eq. (81)}^{21}$$

2.7 Determination of a Convection Coefficient

2.7.1 Free Convection

Due to the quiescent nature of this application, only free convection should be considered. In very sensitive cases, transport theory methods can be employed to predict velocities of fluid films; however, these will not be discussed here. To determine a free convection coefficient, we recognize the Grashof number, a ratio of buoyancy forces to viscous forces, expressed as:

$$Gr_L = \frac{g\beta(T_s - T_\infty)L_c^3}{\nu^2} \quad \text{Eq. (82)}$$

The characteristic length is given as,

$$L_c = \frac{V}{A_s} \quad \text{Eq. (83)}$$

Where, A_s and V are surface area and Volume, respectively. This dimensionless parameter is to free convection as the Reynolds number is to forced convection.

²⁰ $Jkg^{-1}^\circ C^{-1}$ and the curve fit $R^2 = 1$

²¹ $Wm^{-1}^\circ C^{-1}$ and the curve fit $R^2 = 1$

A simplification of our case is possibly analogous to the special case of a vertical surface in an infinite and quiescent medium [46]. For this case, we will need to calculate the Prandtl number.

$$Pr \equiv \frac{\nu}{\alpha} = \frac{c_p \mu}{k} \quad \text{Eq. (84)}$$

The dimensionless surface temperature gradient is a function of the Prandtl number [46] and is expressed as:

$$T^* = f(gPr) \quad \text{Eq. (85)}$$

And can be approximated as,

$$gPr = \frac{0.75Pr^{1/2}}{\left(0.609 + 1.221Pr^{1/2} + 1.238Pr\right)^{1/4}} \quad \text{Eq. (86)}$$

By utilizing Newton's Law of Cooling, the localized Nusselt number can be written as [46]:

$$Nu = \frac{hL}{k} = \frac{\left[q''_s / (T_s - T_\infty)\right] x}{k} \quad \text{Eq. (87)}$$

Additionally, using Fourier's Law to describe the surface temperature as a gradient with respect to the similarity variable, we can express the heat flux as [46]:

$$q''_s = -k \frac{\partial T}{\partial y} \Big|_{y=0} = -\frac{k}{x} (T_s - T_\infty) \left(\frac{Gr_x}{4}\right)^{1/4} \frac{dT^*}{d\eta} \Big|_{\eta=0} \quad \text{Eq. (88)}$$

Where, η is the similarity variable as obtained by Ostrach [48],

$$\eta \equiv \frac{y}{x} \left(\frac{Gr_x}{4}\right)^{1/4} \quad \text{Eq. (89)}$$

With this, Equation 87 can be idealized and rearranged to solve for a convection coefficient.

$$h = \frac{\left(\frac{Gr_x}{4}\right)^{1/4} (gPr)k}{x} \quad \text{Eq. (90)}$$

This convection coefficient can be confirmed with employment of the Rayleigh number and its relationship to the Nusselt and Prandtl numbers as suggested by Churchill and Chu [46].

$$Ra = GrPr \quad \text{Eq. (91)}$$

$$Nu = \left\{ 0.825 + \frac{0.387Ra^{1/6}}{\left[1 + \left(\frac{0.492}{Pr} \right)^{9/16} \right]^{8/27}} \right\}^2 \quad \text{Eq. (92)}$$

We can then utilize the definition of the Nusselt number to find the convection coefficient.

$$Nu \equiv \frac{hL}{k_f} \quad \text{Eq. (93)}$$

It is always worthwhile to quickly calculate the Biot number to determine if the lumped capacitance methods can be employed²².

$$Bi \equiv \frac{hL}{k} \quad \text{Eq. (94)}$$

2.8 Theoretical Solutions to Thermal Analysis

2.8.1 Constant Surface Convection

Treating our case as an instance of constant surface convection, we can solve for the body temperature at time, t and distance, x .

$$\frac{T(x,t) - T_i}{T_\infty - T_i} = \text{erfc} \left(\frac{x}{2\sqrt{\alpha t}} \right) - \left[\exp \left(\frac{hx}{k} + \frac{h^2 \alpha t}{k^2} \right) \right] \left[\text{erfc} \left(\frac{x}{2\sqrt{\alpha t}} + \frac{h\sqrt{\alpha t}}{k} \right) \right] \quad \text{Eq. (95)}$$

²² Valid only when, $Bi \leq 0.1$.

2.8.2 Constant Surface Temperature

For the case where a fluid medium and body surface experience a rate of heat transfer such that the body surface instantaneously achieves the fluid temperature, such that $T_s = T_\infty$ and $h = \infty$, the temperature gradient may be evaluated as though the body is experiencing a constant surface temperature. This constant surface temperature case is evaluated as:

$$\frac{T(x, t) - T_s}{T_i - T_s} = \operatorname{erf}\left(\frac{x}{2\sqrt{\alpha t}}\right) \quad \text{Eq. (96)}$$

These solutions are valid for the idealized case of a semi-infinite solid of thickness $2L$ and at Fourier numbers less than 0.2. Mathematically, that is,

$$Fo = \frac{\alpha t}{L_c^2} \leq 0.2 \quad \text{Eq. (97)}$$

The following figure shows results for a sample calculation using the above formulations. The body had an initial temperature of 20°C and was surrounded by a quiescent fluid at 450°C. The materials are steel and zinc.

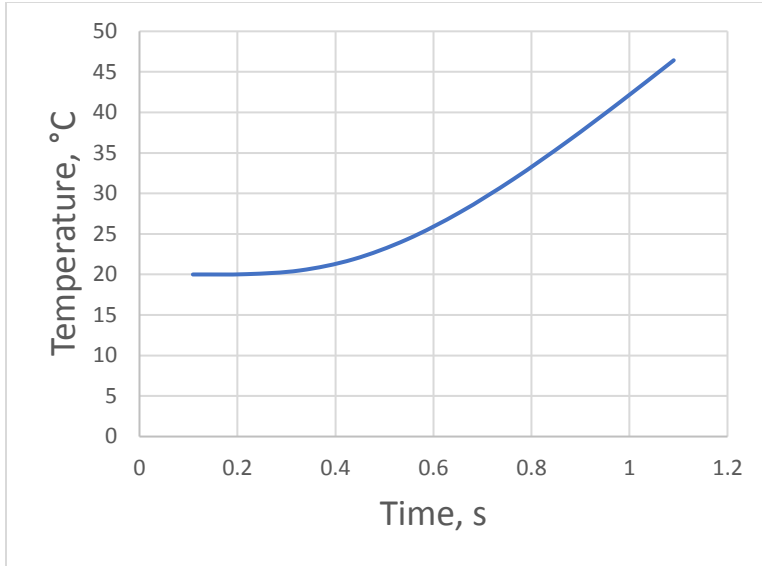


Figure 2.24 Temperature rise in a solid body exposed to constant surface convection

2.8.3 Exact and Approximate Solutions to Transient Conduction

If we consider a thin section, one whose wall thickness can be described as small compared with its length and width, it follows that we can assume conduction is taking place in one direction only. Looking at our case of hot-dip galvanizing, the scenario can be described as a material at some temperature at time zero which is immersed in a fluid of unequal temperature. Furthermore, we can assume that the convection conditions are the same on all the boundary conditions and therefore symmetric about the midplane. The exact solution to this problem is as follows (published values of C_n and ζ_n are shown in Table 2.7 on the following page).

$$\theta^* = \sum_{n=1}^{\infty} C_n \exp(-\zeta_n^2 Fo) \cos(\zeta_n x^*) \quad \text{Eq. (98)}$$

Where,

$$C_n = \frac{4 \sin(\zeta_n)}{2\zeta_n + \sin(2\zeta_n)} \quad \text{Eq. (99)}$$

The values of ζ_n are the discrete solutions of the transcendental equation:

$$Bi = \zeta_n \tan(\zeta_n)$$

Eq. (100)

Table 2.7 Tabulated values of C_n and ζ_n

Bi	ζ_n	C_n
0.01	0.0998	1.0017
0.02	0.141	1.0033
0.03	0.1723	1.0049
0.04	0.1987	1.0066
0.05	0.2218	1.0082
0.06	0.2425	1.0098
0.07	0.2615	1.0114
0.08	0.2791	1.013
0.09	0.2956	1.045
0.1	0.3111	1.0161
0.15	0.3779	1.0237
0.2	0.4328	1.0311
0.25	0.4801	1.0382
0.3	0.5218	1.045
0.4	0.5932	1.058
0.5	0.6533	1.0701
0.6	0.7051	1.0814
0.7	0.7506	1.0919
0.8	0.791	1.1016
0.9	0.8274	1.1107
1	0.8603	1.1191
2	1.0769	1.1785
3	1.1925	1.2102
4	1.2646	1.2287
5	1.3138	1.2402
6	1.3496	1.2479
7	1.3766	1.2532
8	1.3978	1.257
9	1.4149	1.2598
10	1.4289	1.262
20	1.4961	1.2699
30	1.5202	1.2717
40	1.5325	1.2723
50	1.54	1.2727
100	1.5552	1.2731
∞	1.5708	1.2733

For Fourier numbers greater than 0.2, and at the midplane of a symmetric element, the following is an approximate solution.

$$\theta_o^* = C_1 \exp(-\zeta_n^2 Fo) \quad \text{Eq. (101)}$$

Where,

$$\theta_o^* = \frac{\theta^*}{\cos(\zeta_n x^*)} \quad \text{Eq. (102)}$$

Where at the midplane,

$$\begin{aligned} x^* &= 0, \\ \therefore \theta_o^* &= \theta^* \end{aligned}$$

2.8.4 Sample Finite Element Thermal Analysis

Transient Study with Free Convection Using Finite Element Analysis Software

To create a valid sample analysis using the case for a semi-infinite body, we define a time step criterion to meet the restriction for the Fourier number. Where, n is the desired number of steps.

$$\Delta t = \frac{0.2 L_c^2 \alpha^{-1}}{n} \quad \text{Eq. (103)}$$

For some cases, the finite element analysis software requires a specific time constant or specific characteristic time to ensure stable results.

$$\Delta t = \frac{L_c^2}{\alpha} \quad \text{Eq. (104)}$$

This time constant, however, may result in Fourier numbers larger than 0.2.

Sample Solution for Constant Surface Convection

Using the same convection and temperature parameters as previously mentioned resulted in a very similar result as with the theoretical method. The result from the semi-infinite case was, 115.567°F @ 1.09sec and the result of the FEA simulation was, 117.531°F @ 1.09sec ²³.

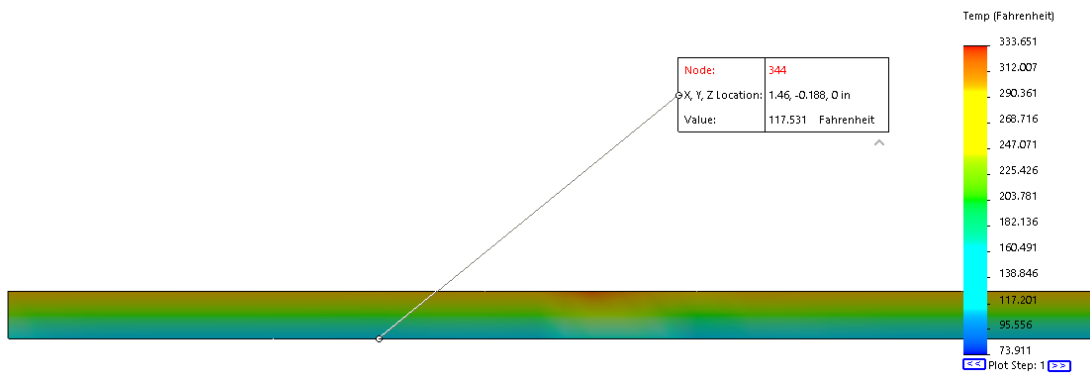


Figure 2.25 Result of sample FEA study

Application of Concepts

To set up the finite element method (FEM) as shown in Figure 1.2 Analysis showing stresses in a structure with high restraint, we need to determine the applicable boundary condition. To do this, we will use an exact solution to determine the time to reach the bath temperature. To solve for this period, we will evaluate a structural member in a two-dimensional plane to simplify calculations. Next, we need to calculate the thermomechanical properties of both the zinc and the steel for our model. By utilizing Equation 72, we take the thermal conductivity of the heated steel to be the average value over the temperature range of $T_i=75^{\circ}\text{F}$ and $T_{\infty}=840^{\circ}\text{F}$ resulting in $k=0.00057194$ Btu/(s·in·°F). By using Equation 74 through Equation

²³ The average result was, 116.793°F @ 1.09sec .

93, we calculate the thermophysical properties of zinc at $T_{\infty}=840^{\circ}\text{F}$. The primary outcome of these calculations is the thermal convection coefficient and thermal diffusivity. These parameters are, $h=0.011018762 \text{ Btu}/(\text{s}\cdot\text{in}^2\cdot^{\circ}\text{F})$ and $\alpha=0.044261129 \text{ in}^2/\text{s}$, respectively.

From Equation 94 we calculate the Biot number as $(L = \sqrt[3]{16}/2 = 0.09375\text{in})$,

$$Bi = \frac{0.011 \times 0.09375}{0.00057} = 1.807$$

The Fourier number is calculated as ($@t = 2.6596\text{sec}$):

$$Fo = \frac{0.0443 \times 2.66}{0.09375^2} = 13.4$$

Utilizing Equation 101 yields,

$$\theta^* = 1.167e^{-(1.04^2)13.4} = 6.8 \times 10^{-7}$$

Finally, we can verify this with Equation 105,

$$\theta^* = \frac{T_0 - T_{\infty}}{T_i - T_{\infty}} \quad \text{Eq. (105)}$$

$$T(0, 2.66\text{sec}) = 840 + 6.8 \times 10^{-7}(75 - 840) = 839.99^{\circ}\text{F}$$

From this we can see that the temperature change is extremely rapid. In true application, the period for dipping is roughly 8 minutes with an additional 8 minutes fully submerged in the tank and approximately 7 to 10 minutes to remove the structure from the tank. Given that the structure will certainly be held in the tank for a period much greater than 2.66 seconds, the boundary condition selected for the FEM model will be one of constant surface temperature.

CHAPTER 3

FINITE ELEMENT ANALYSIS OF A NEW DESIGN

3.1 Design for Hot-Dip Galvanizing

3.1.1 Design Logic

The trailers thermal design considerations are hinged on the basis of restraint as described in AWS D1.1 Annex H. The fewer the degrees of freedom, the higher the level of restraint. This restraint is directly related to the stresses developed in a material during thermal expansion. As material is heated, either by welding procedures or hot-dip galvanizing, it will tend to deflect or otherwise deform due to the effects of thermal expansion. The formulas for calculating free thermal expansion in solids are as follows.

$$\text{Linear} \quad \delta_T = \alpha_T \Delta T L_0 \quad \text{Eq. (106)}$$

$$\text{Area} \quad \delta_T = 2\alpha_T \Delta T A_0 \quad \text{Eq. (107)}$$

$$\text{Volumetric} \quad \delta_T = 3\alpha_T \Delta T V_0 \quad \text{Eq. (108)}$$

If the solid is restricted from movement, high internal stress can develop. The relationship between linear expansion and the internal reaction of the member is:

$$\alpha_T \Delta T L_0 = \frac{P L_0}{EA} \quad \text{Eq. (109)}$$

Using our previously defined relationship between force and stress we can relate the stress as a thermal effect.

$$\sigma = \alpha_T \Delta T E \quad \text{Eq. (110)}$$

Calculating the internal force involves a simple rearrangement of this.

$$P = \alpha_T \Delta T E A \quad \text{Eq. (111)}$$

With respect to hot-dip galvanizing, there are three primary cases for consideration: As the weldment is being lowered into the tank and is not totally engulfed in the liquid zinc; the weldment is completely in the tank and all the material is exposed to the same boundary conditions; as the weldment is removed from the tank and some portion of the material remains in the zinc bath. A potential outcome of this analysis is to indicate the likelihood of LMAC verse failure due simply to distortion in primary structural elements induced from temperature gradients. Failure can be defined as any mechanical failure or distortion such that any one part would no longer qualify under ASTM A6.

3.1.2 Design Comparison

The original design was constructed primary of hollow structural section (HSS) rectangular tubing (TR). This design has very high restraint which results in the stresses shown in Figure 3.7 when subjected to the thermal loads during hot-dip galvanizing. A simplified version of this design is shown.

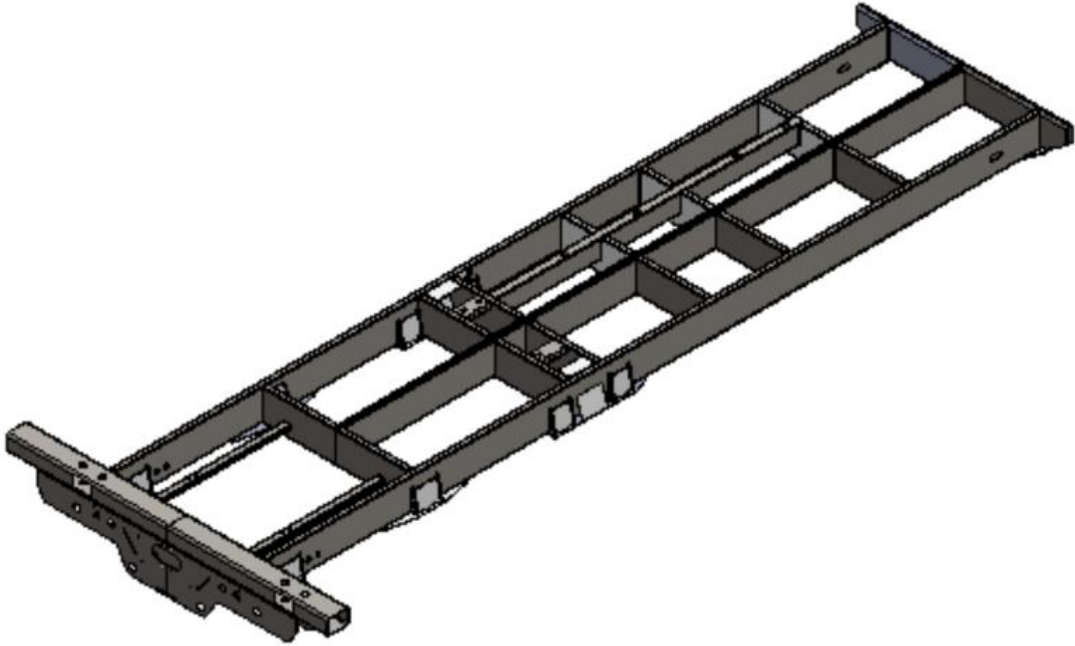


Figure 3.1 Simplified model of original design

We can clearly see that all the joints along the center beam element are held in restraint by the outer beams and the connecting elements. The new design (Figure 3.2) concept utilizes stronger elements and therefore requires less bracing. This naturally reduces the level of restraint in the structure while allowing it to carry the same load. Additionally, because there are no hollow sections, the zinc is able to freely flow over this structure which reduces the value of \mathbb{D} in Equation 54.

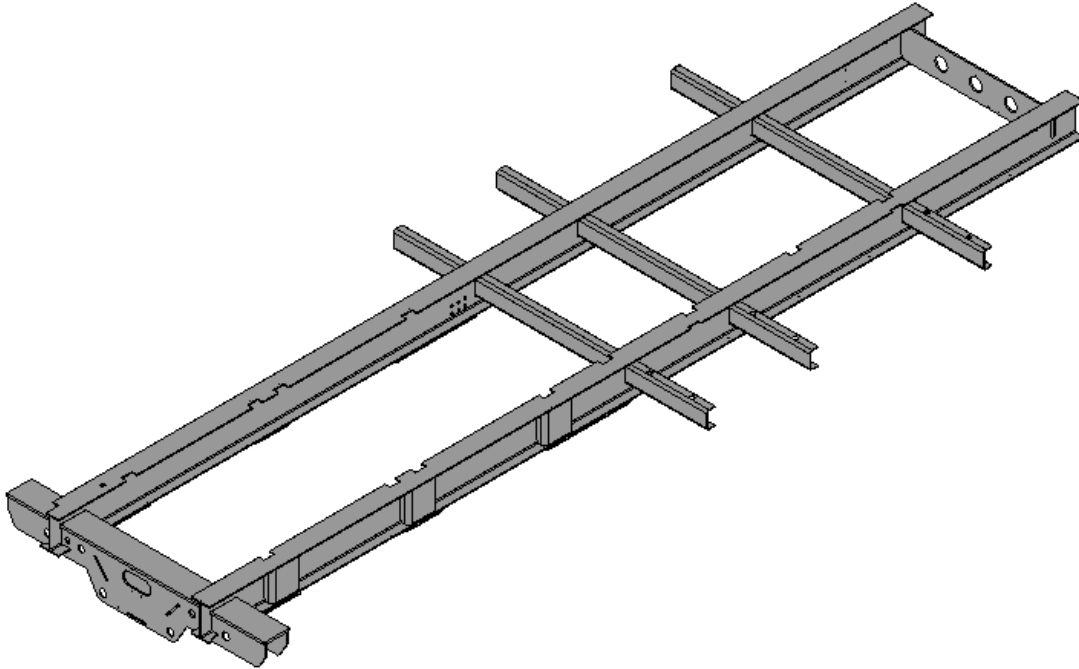


Figure 3.2 Simplified model of new design

3.1.3 Thermal Analysis of Designs

The failure in the first design which ultimately prompted this research, was likely due to the structures high level of restraint and having to be “double” dipped during galvanizing. That is to say, the galvanizing tank was too small to accommodate the entire frame and therefore half the frame was dipped and removed from the tank and the process repeated for the other half. To adequately compare the two designs, the same boundary conditions must be applied to each structure. Due to restrictions in computing power, one thermal load case is selected on the basis of it being the worst-case scenario.

The structure is modelled halfway dipped in a material and held in place for four minutes. A simple graphic can explain the significance of using this scenario. As a portion of the steel becomes heated, it will expand due to the rules of thermal expansion; however, the portion of the steel that is unheated does not wish to expand. Therefore, the expanded steel experiences a force

attempting to keep it from expanding, while the cooler steel experiences a tensile force exerted on it by the expanding heated steel.

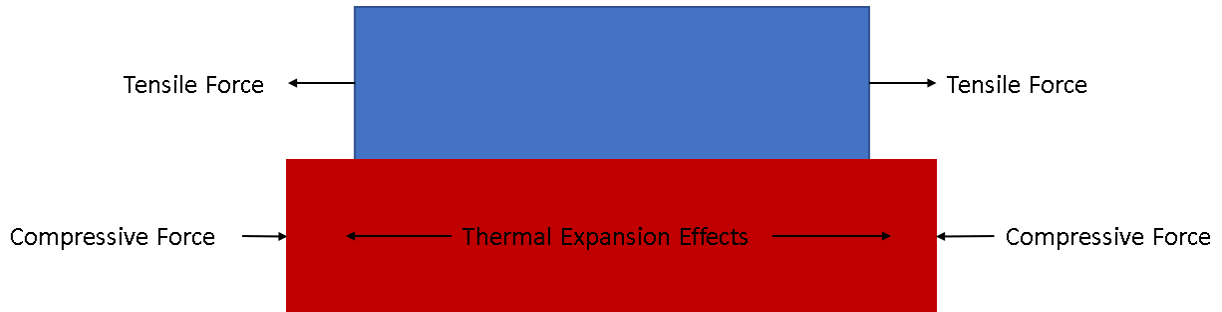


Figure 3.3 Graphic of boundary condition effects

The simulation is done in two stages: First; a transient thermal study and second, a static stress analysis. For the thermal analysis, steel properties were selected as A500 Gr. B for the first structure and A572 Gr. 50 for the second structure. The properties are at room temperature for both steels. Properties of zinc were calculated as previously described by Equations 74 through 81. The sides and bottom of the “tank” are held at a constant temperature and the exposed surfaces of the steel and the top surface of the tank are exposed to free convection with air at 85°F in a quiescent condition. Prior to getting dipped, steels are dipped in cleaning and flux solutions; also, at elevated temperatures. The initial temperature of the steel is therefore set to 150°F and the zinc bath has an initial temperature of 840°F. It should be noted that turbulent flow induced from the temperature gradient in the boundary layers is neglected.

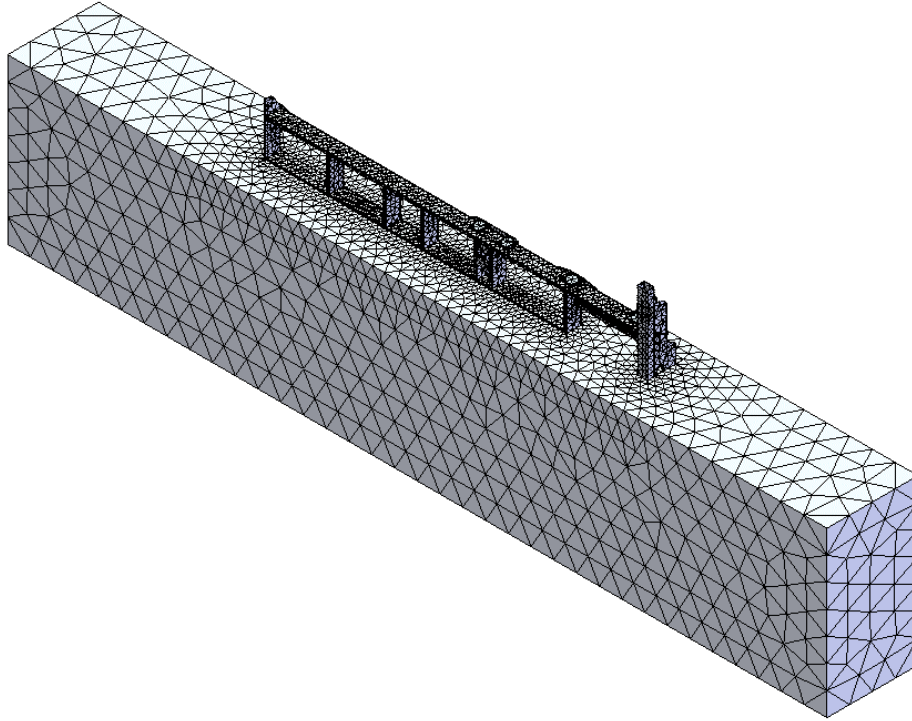


Figure 3.4 Model of first design halfway dipped in galvanizing bath

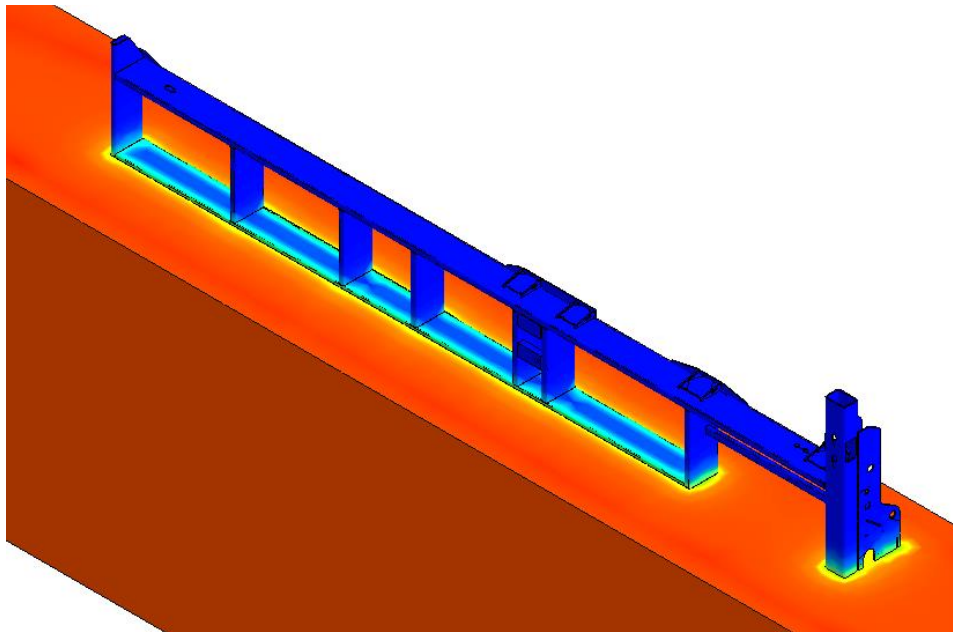


Figure 3.5 Resulting temperature gradients from thermal study of first design

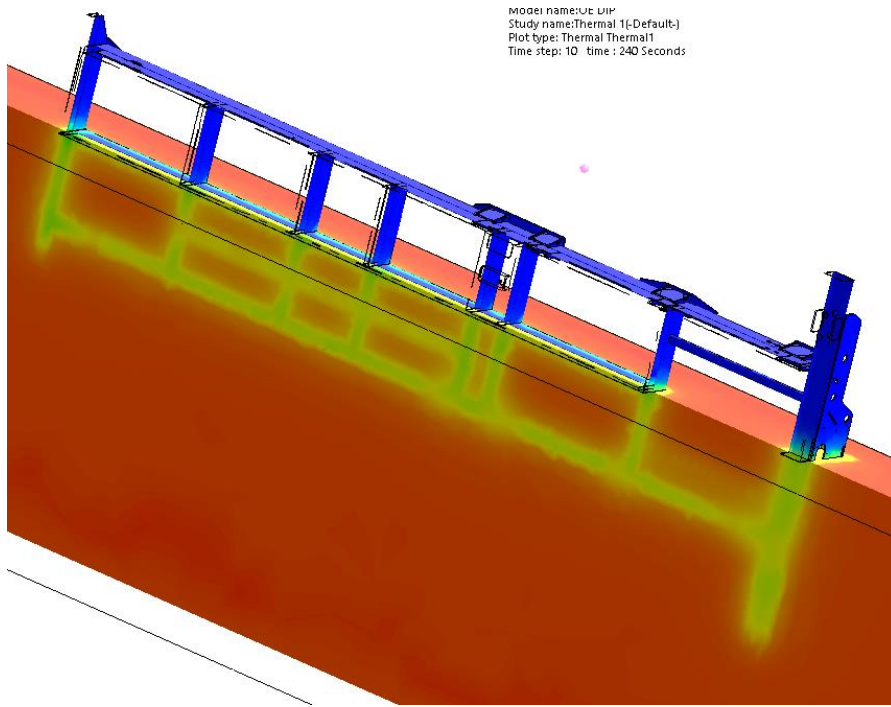


Figure 3.6 Cut section of resulting temperature gradients from thermal study of first design

The static stress analysis is set up to exclude the zinc body. The study was conducted once with a spring load applied to the outer surfaces of the frame to replicate the tension in the liquid and once without such a fixture and the differences were negligible. Therefore, to be more efficient with computational resources, this tension was removed for the final study. The only load applied was the thermal load from last step of the thermal study and inertial effects are ignored. The mechanical properties of A500 Gr. B at these temperatures are taken as: $\sigma_y = 37,128psi$, $UTS = 51,272psi$ and $E = 18,386ksi$. These values are calculated by linear interpolation of the AISC method. Thermophysical properties are calculated as mentioned previously.

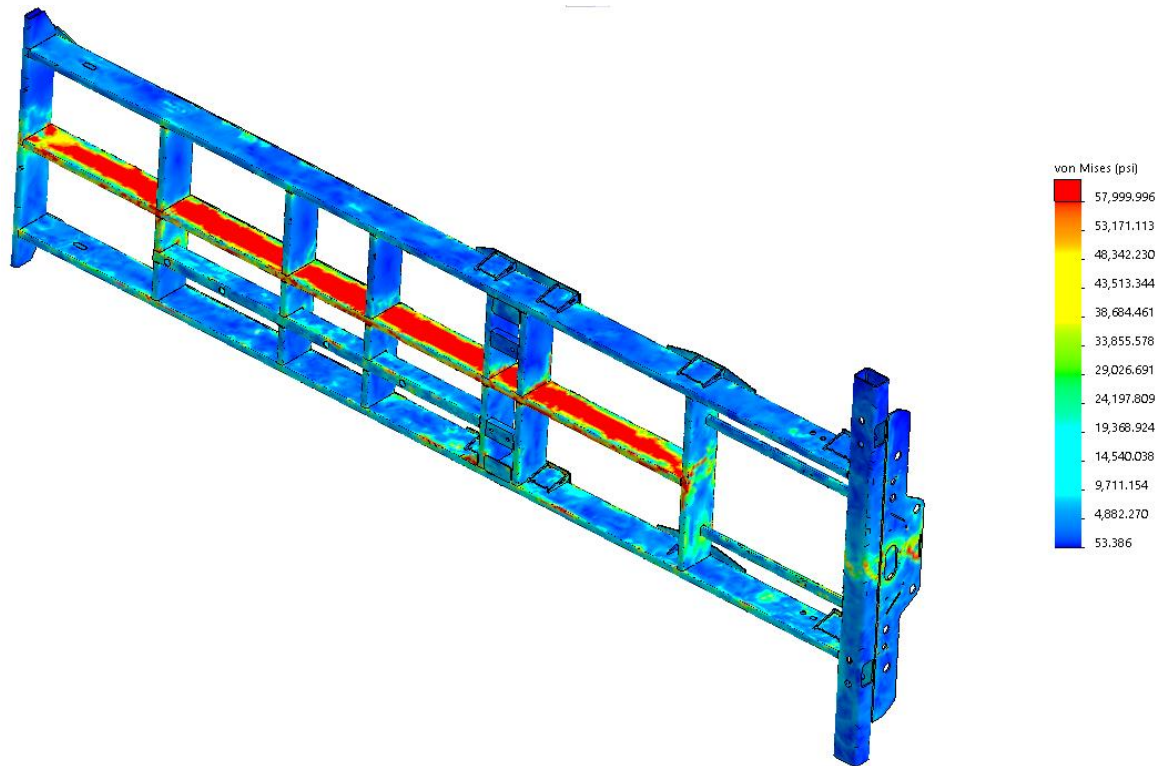


Figure 3.7 Thermally induced stresses in first structure

It is important to note that the stresses above yield cannot be taken as totally accurate. This is because, as previously described, Hooke's Law no longer applies; however, since the software is doing a linear analysis, it is still utilizing this relationship to report stress values.

The new design was analyzed in the same fashion and the results are as shown. The primary difference was the steel selected. Whereas the original design utilized A500 Grade B steel, the new design is constructed mostly of plate steel and structural shapes and therefore, a greater variety of material options are available. A572 Grade 50 steel is chosen and the properties at elevated temperatures are evaluated as $\sigma_y = 44,200psi$, $UTS = 57,460psi$ and $E = 18,386ksi$.

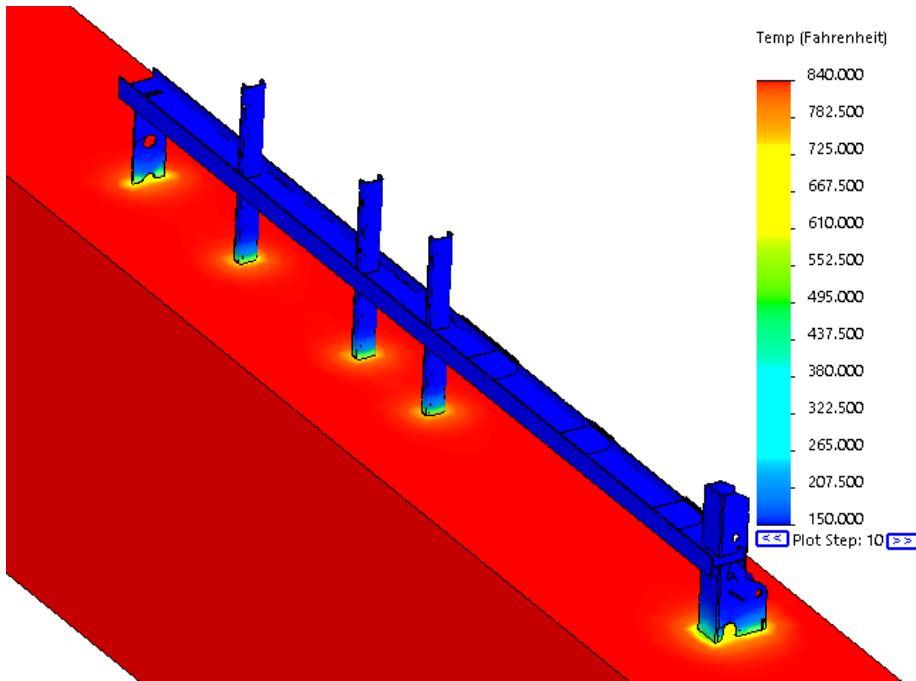


Figure 3.8 Results from thermal study on new design

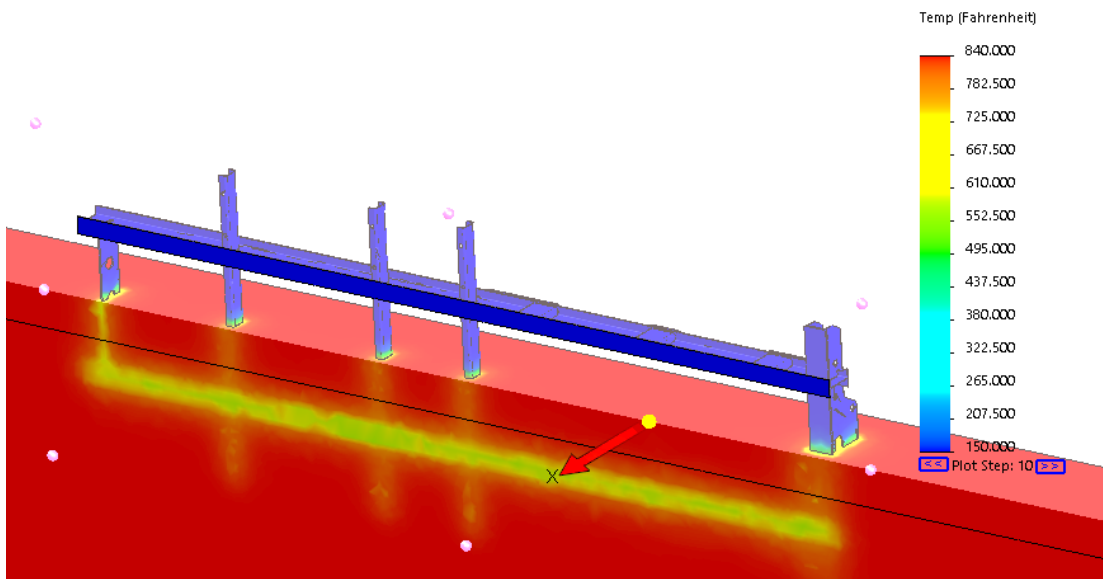


Figure 3.9 Cut section of thermal results on new design

It is interesting to note here, the temperature of the cut sections. They are much lower than the mathematically calculated values. A potential explanation for this, is because mathematically, as

the change in temperature gets closer to zero, the solution goes to infinity and therefore the results are ineffective at portraying what is actually going to happen.

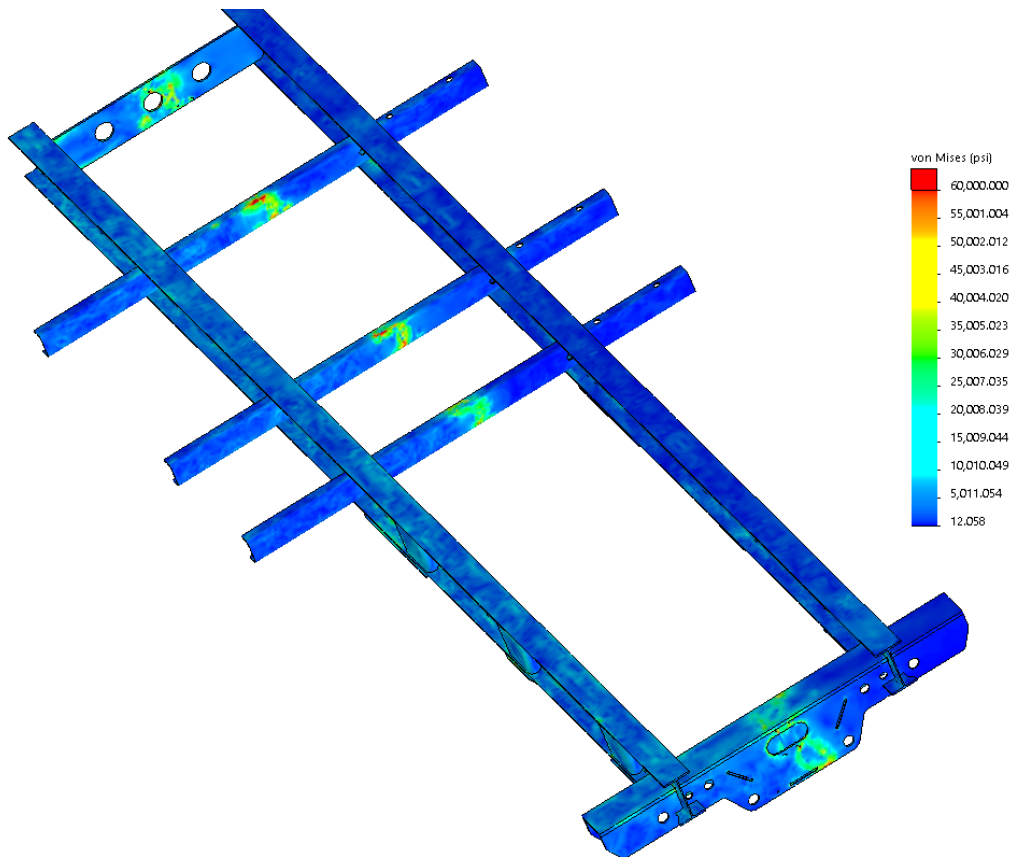


Figure 3.10 Results from stress analysis on new design

We can see a clear reduction in stress. This is likely because the structure is allowed to move to such an extent that the relative displacement of its member has little to no adverse effect on the structure as a whole. Finally, we look at the results of an actual structure designed to these guidelines post hot-dip galvanizing. The new design was hot-dipped at a facility with a tank large enough to fully submerge the frame in a single dip. It took approximately eight minutes to fully submerge the frame. At which time it remained in the bath for another eight minutes. Finally, over a period of seven minutes, the frame was removed from the tank. Permanent deformation

occurred in one of the plates towards the front of the trailer, but this plate is not structural and was not included in the simulation analysis. There were no failures in any element on the structure that were included in the analysis. A more comprehensive analysis will be completed to replicate the deformed plate. In the mean-time, gusseting has proven to be an effective method to mitigate warpage in non-structural components.



Figure 3.11 New design post hot-dip galvanizing (shared with permission from Valmont)



Figure 3.12 New design post hot-dip galvanizing (shared with permission from Valmont)

CHAPTER 4

CONCLUSIONS AND FUTURE WORK

What one can draw from this report, is the clear affect joint restriction and compliance to galvanizing design recommendations have on the feasibility of hot-dip galvanizing a welded structure. We see that high stresses resulted during just a “single” dip and while there exists no doubt about the negative consequence of double-dipping, this was not necessarily the cause of failure. The size of the structure is a limiting factor in practical testing to validate these results. Because we are analyzing the structures with a linear approach, it is obvious that the greater the length, the greater the expansive effect will be and therefore we can hypothesize that smaller, shorter structures will not behave in a similar manner.

More work needs to be done to fully and precisely understand the mechanisms described herein. Despite this, we were able to analyze the structures with FEM software and receive results equivalent to the real-world application. This can then be considered as an analysis process control, and while it will always require some fine-tuning, this FEA process can be used to confidently analyze future designs. Adjustment will come in the form of layering transient studies to get a more accurate result and using more complicated geometries which exist in the real world. Additionally, as properties at elevated temperatures become better understood, these parameters will continue to be updated in the FEM model. Later revisions of this paper will aim to include the discussions on the logic in setting up the FEA appropriately, better test methods to measure strain directly during hot-dip galvanizing and guidelines for mechanical testing.

Eventually, a database of empirical data will be available as a design aid which is more accessible than complex analytical methods.

REFERENCES

- [1] The British Constructional Steelwork Association, Ltd., "Galvanizing Structural Steelwork An Approach to the management of Liquid Metal Assisted Cracking," The British Constructional Steelwork Association, Ltd., London.

- [2] G. E. Dieter, Jr, Mechanical Metallurgy, New York: McGraw-Hill Book Company, 1961.

- [3] R. H. Wagoner and J.-L. Chenot, Fundamental of Metal Forming, New York: John Wiley & Sons, Inc., 1997.

- [4] S. T. Rolfe, "Fracture and Fatigue Control in Structures," *Engineering Journal/American Institute of Steel Construction*, no. First Quarter, 1980.

- [5] W. J. P. Becker, "Ductile and Brittle Fracture," in *Principles of Failure Analysis* , Materials Park, ASM International, 2002.

- [6] W. F. Smith and J. Hashemi, "Mechanical Properties of Materials," in *Foundations of Material Science and Engineering*, 4 ed., New York, The McGraw-Hill Companies, Inc., 2006, pp. 279-293.

- [7] J. M. Barson and R. T. Stanley, Fracture and Fatigue Control in Structures, 3 ed., West Conshohocken: ASTM, 1999.

- [8] ASM International, "Parameters for Estimating Fatigue Life," in *ASM Handbook Fatigue and Fracture*, vol. 19, S. R. Lampman, Ed., Materials Park, ASM International, 1996.

- [9] S. Mason, "Fatigue: A Complex Subject - Some Simple Approximations," National Aeronautics and Space Administration, Cleveland, 1964.

- [10] T. Jefferson, *Metals and How to Weld Them*, Cleveland: The James F. Lincoln Arc Welding Foundation, 1990.
- [11] American Welding Society A2 Committee on Definitions and Symbols, "AWS A2.4 - Standard Symbols for Welding, Brazing, and Nondestructive Examination," American Welding Society Board of Directors, Miami, 2007.
- [12] American Welding Society D1 Committee, "AWS D1.3/D1.3M:2018," American Welding Society Board of Directors, Miami, 2018.
- [13] D. K. Miller, Sc.D., P.E., "Consider Direction of Loading When Sizing Fillet Welds," *Welding Innovation*, vol. XV, no. 2, 1998.
- [14] American Institute of Steel Construction, "Design Considerations for Welds," in *Steel Construction Manual*, 13 ed., American Institute of Steel Construction, 2005, pp. 8-8.
- [15] AWS Committee on Structural Welding, "AWS D1.1 Structural Welding Code - Steel," AWS Board of Directors, Miami, 2015.
- [16] T. Kasuya and N. Yurioka, "Carbon Equivalent and Multiplying Factor For Hardenability of Steel," in *72nd Annual AWS Meeting*, Detroit, 1991.
- [17] A. C. A01, "A992/A992M-11," ASTM International, West Conshohoken, 2015.
- [18] G. E. Linnert, *Welding Metallurgy, Carbon and Alloy Steels*, vol. 1, American Welding Society, 1965.
- [19] P. Pinhero and Y. Zhou, "Welding," in *Smithells Metals Reference Book*, 8 ed., W. P. Gale and T. P. Totenmeier, Eds., Kidlington, Butterworth-Heinemann, 2004, pp. 33-19.
- [20] ASM International, *Properties and Selection: Iron, Steels, and High-Performance Alloys*, vol. 1, Materials Park: ASM International, 1990.

- [21] M. F. Ashby, *Materials Selection in Mechanical Design*, 4 ed., Burlington: Butterworth-Heinemann, 2011.
- [22] E. Oberg, J. D. Franklin, H. L. Horton and H. H. Ryffel, "Bending Sheet Metal," in *Machinery's Handbook*, 30 ed., South Norwalk, Industrial Press, Inc., 2016, p. 1374.
- [23] ArcelorMittal USA, "Guidelines for fabricating and processing plate steel," ArcelorMittal USA, Burns Harbor, IN; Coateville, PA; Conshohocken, PA.
- [24] V. P. Boljanovic, *Sheet Metal Forming Processes and Die Design*, New York: Industrial Press, Inc., 2004.
- [25] ASTM Committee A01, "A1011/A1011M-18a," ASTM International, West Conshohocken, 2019.
- [26] ASTM Committee A01, "A36/A36M-14," ASTM International, West Conshohocken, 2019.
- [27] ASTM Committee A01, "A572/A572M-18," ASTM International, West Conshohocken, 2019.
- [28] W. F. Smith and J. Hashemi, "Corrosion," in *Foundations of Materials Science and Engineering*, 4 ed., New York, The McGraw-Hill Companies, Inc., 2006, pp. 758-759.
- [29] T. J. Kinstler, "Current Knowledge of the Cracking of Steels During Galvanizing," GalvaScience LLC, Springville.
- [30] J. Poag and J. Zervoudis, "Influence of Various Parameters on Steel Cracking During Galvanizing," in *Presented at the AGA Tech Forum*, Kansas City, 2003.
- [31] G. W. Dallin, "Continuous Hot-Dip Galvanizing - Process and Products," International Zinc Association, 2015.

- [32] ASTM Committee A05, "A 123A/A 123M Standard Specification for Zinc (Hot-Dip Galvanized) Coatings on Iron and Steel Products," ASTM International, West Conshohocken, 2002.
- [33] B. A. Duran III, "Silicon Content of Steel," American Galvanizers Association, Centennial, 2012.
- [34] ASTM Committee A05, "ASTM 385/A385M-17 Standard Practice for Providing High Quality Zinc Coatings (Hot-Dip)," ASTM International, West Conshohocken, 2017.
- [35] H. J. Grabke and E. Reicke, "Absorption and Diffusion of Hydrogen in Steels," Max-Planck-Institut für Eisenforschung GmbH, Dusseldorf, 2000.
- [36] S. J. Kim, D. W. Yun, H. G. Jung and K. Y. Kim, "Determination of Hydrogen Diffusion Parameters of Ferritic Steel from Electrochemical Permeation Measurement under Tensile Loads," Electrochemical Society, 2014.
- [37] M. Meyers and K. Chawla, "Environmentally Assisted Fracture in Metals," in *Mechanical Behavior of Materials*, 2 ed., New York, Cambridge University Press, 2009, pp. 824-830.
- [38] American Institute of Steel Construction, "Specifications for Structural Steel Buildings," in *Steel Construction Manual*, 13 ed., American Institute of Steel Construction, 2005, pp. 16.1-v - 16.3-68.
- [39] J. A. Milke, "Analytical Methods for Determining Fire Resistance of Steel Members," in *SFPE Handbook of Fire Protection Engineering*, 3 ed., Quincy, Massachusetts: National Fire Protections Association, Inc. , 2002, pp. 1167-1196.
- [40] ASCE Committee on Fire Protection, Structural Division, American Society of Civil Engineers, Structural Fire Protection, New York: The American Society of Civil Engineers, 1992.
- [41] T. Lie and W. Stanzak, "Emperical Method for Calculating Fire Resistance of Protected Steel Columns," *Engineering Journal*, vol. 57, no. 5/6, p. 73, 1975.

- [42] W. E. Luecke, D. J. McColskey, C. N. McCowan, S. W. Banovic, R. J. Fields, T. A. Foecke and F. W. Gayle, *Mechanical Properties of Structural Steel*, Washington: U.S. Government Printing Office, 2005, p. 46.
- [43] M. J. Assael, I. J. Armyra, J. Brillo, S. V. Stankus, J. Wu and W. R. Wakeham, "Reference Data for the Density and Viscosity of Liquid Cadmium, Cobalt, Gallium, Indium, Mercury, Silicon, Thallium, and Zinc," *American Institute of Physics*, 2012.
- [44] A. Xian, L. Wang and H. Shao, "Density Measurement of Liquid Indium and Zinc by the γ -Ray Attenuation Method," *Pion*, 2006.
- [45] S. Bakhtiyarov, "The Physical Properties of Pure Metals At Elevated Temperatures," in *Smithells Metals Reference Book*, Burlington, Butterworth-Heinemann, 2004, pp. 14-7.
- [46] T. L. Bergman, A. S. Lavine, F. P. Incropera and D. P. Dewitt, "Free Convection," in *Fundamentals of Heat and Mass Transfer*, John Wiley & Sons, Inc, 2011, pp. 594-601.
- [47] W. Gale and T. Totemeier, Eds., *Smithells Metals Reference Book*, 8 ed., Burlington: Butterworth-Heinemann, 2004.
- [48] S. Ostrach, "Natural Convection in Enclosures," *Advances in Heat Transfer*, vol. 8, pp. 161-227, 1972.
- [49] W. C. Young, R. G. Budynas and A. M. Sadegh, "Torsion," in *Roark's Formulas for Stress and Strain*, 8 ed., New York, The McGraw Hill Companies, 2012, pp. 401-444.
- [50] A. N. Gent and J. D. Walter, "The Pneumatic Tire," U.S. Department of Transportation, National Highway Traffic Safety Administration, Washington D.C., 2006.
- [51] "Spring Design," in *Machinery's Handbook*, 30 ed., Industrial Press.
- [52] R. Hibbeler, *Statics and Mechanics of Materials*, 4 ed., Upper Saddle River: Pearson Prentice Hall, 2014, p. 525.

- [53] G. C. Zoerb, "SR-4 Strain Gage Instrumentation For Power Measurement," Agricultural Engineering Department, South Dakota State College, Brookings.
- [54] A. J. Wheeler and G. R. Ahmad, Introduction to Engineering Experimentation, Upper Saddle River: Pearson Higher Education, 2010, p. 249.
- [55] D. Ashlock and A. Warren, *The Engineer's Guide to Signal Conditioning*, National Instrument, 2015.
- [56] Omega, *Practical Strain Gage Measurements*, Agilent Technologies Inc., 199.
- [57] Federal Motor Carrier Safety Administration, "Subtitle B, Chapter 3, Subchapter B, Part §390," in *Title 49*, 2019.

APPENDIX A

RELEVANT PROPERTIES OF LOAD BEARING MEMBERS

A.1 Calculations for Main Beam Selection

A.1.1 Requirements

The following are required parameters:

- Flange width;
- flange thickness;
- web height;
- web thickness;
- web radius
- modulus of elasticity/Young's modulus;
- yield strength;
- Poisson's ratio.

A.1.2 Width to Thickness Ratios

Ratios are used to determine whether a beam element qualifies as compact, non-compact or slender. Compactness is a measure of the tendency to experience local buckling. For I-shaped sections, A1.1 and A1.2 were used as reference for these equations. The results for a W10x22 wide flanged beam are shown in Table A1.1.

Table A1.1 Calculated width-to-thickness ratios for W10x22 beams

LW-TR					
	Compact	Non-Compact	Limit	Ratio	Result
Flange Flexural Compression	9.15161188	24.08318916	No Limit	7.99	Compact
Flange Axial Compression	9.15161188	13.48658593	No Limit	7.99	Compact
Web Flexural Compression	90.55279123	137.2741782	243.6	36.88	Compact
Web Axial Compression	N/A	35.88395184	243.6	36.88	Non-Compact

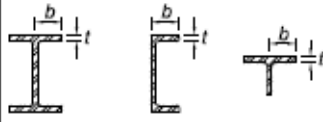
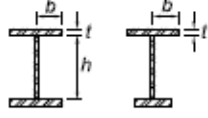
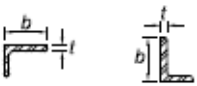
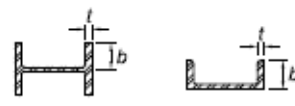
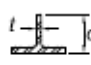
TABLE B4.1b Width-to-Thickness Ratios: Compression Elements Members Subject to Flexure					
Case	Description of Element	Width-to-Thickness Ratio	Limiting Width-to-Thickness Ratio		Examples
			λ_p (compact/ noncompact)	λ_r (noncompact/ slender)	
Unstiffened Elements	10 Flanges of rolled I-shaped sections, channels, and tees	b/t	$0.38 \sqrt{\frac{E}{F_y}}$	$1.0 \sqrt{\frac{E}{F_y}}$	
	11 Flanges of doubly and singly symmetric I-shaped built-up sections	b/t	$0.38 \sqrt{\frac{E}{F_y}}$	$0.95 \sqrt{\frac{k_c E}{F_L}}$ ^{[a] [b]}	
	12 Legs of single angles	b/t	$0.54 \sqrt{\frac{E}{F_y}}$	$0.91 \sqrt{\frac{E}{F_y}}$	
	13 Flanges of all I-shaped sections and channels in flexure about the minor axis	b/t	$0.38 \sqrt{\frac{E}{F_y}}$	$1.0 \sqrt{\frac{E}{F_y}}$	
	14 Stems of tees	d/t	$0.84 \sqrt{\frac{E}{F_y}}$	$1.52 \sqrt{\frac{E}{F_y}}$	

Figure A1.1 Width-to-thickness ratios [42]

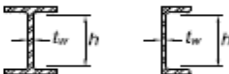
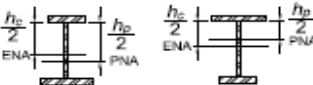
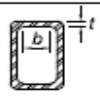
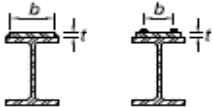
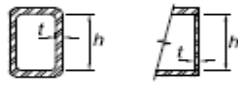
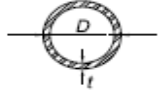
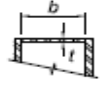
TABLE B4.1b (continued)							
Width-to-Thickness Ratios: Compression Elements Members Subject to Flexure							
Case	Description of Element	Width-to-Thickness Ratio	Limiting Width-to-Thickness Ratio		Examples		
			λ_p (compact/ noncompact)	λ_r (noncompact/ slender)			
Stiffened Elements	15	Webs of doubly symmetric I-shaped sections and channels	h/t_w	$3.76 \sqrt{\frac{E}{F_y}}$	$5.70 \sqrt{\frac{E}{F_y}}$		
	16	Webs of singly symmetric I-shaped sections	h_c/t_w	$\frac{h_c}{h_p} \sqrt{\frac{E}{F_y}}$ [c]	$\left(0.54 \frac{M_p}{M_y} - 0.09\right)^2 \leq \lambda_r$	$5.70 \sqrt{\frac{E}{F_y}}$	
	17	Flanges of rectangular HSS	b/t	$1.12 \sqrt{\frac{E}{F_y}}$	$1.40 \sqrt{\frac{E}{F_y}}$		
	18	Flange cover plates and diaphragm plates between lines of fasteners or welds	b/t	$1.12 \sqrt{\frac{E}{F_y}}$	$1.40 \sqrt{\frac{E}{F_y}}$		
	19	Webs of rectangular HSS and box sections	h/t	$2.42 \sqrt{\frac{E}{F_y}}$	$5.70 \sqrt{\frac{E}{F_y}}$		
	20	Round HSS	D/t	$0.07 \frac{E}{F_y}$	$0.31 \frac{E}{F_y}$		
	21	Flanges of box sections	b/t	$1.12 \sqrt{\frac{E}{F_y}}$	$1.49 \sqrt{\frac{E}{F_y}}$		

Figure A1.2 Width-to-thickness ratios [42]

Qualification of Compact, Non-Compact or Slenderness²⁴

If $\lambda < \lambda_p$ then, Compact
 If $\lambda_p < \lambda < \lambda_r$ then, Non – Compact
 If $\lambda_r < \lambda$ then, Slender

²⁴ Slender sections are to be avoided for structural use in mainframe design.

A.1.3 Relevant Section Properties²⁵ [49]

For the purposes of this thesis, rotation about the x-axis is in the strong direction of the beam while rotation about the y-axis is in the weak direction of the beam. These directions are indicated with subscripts in Equations 112 through 126. Use Figure A1.3 for reference.

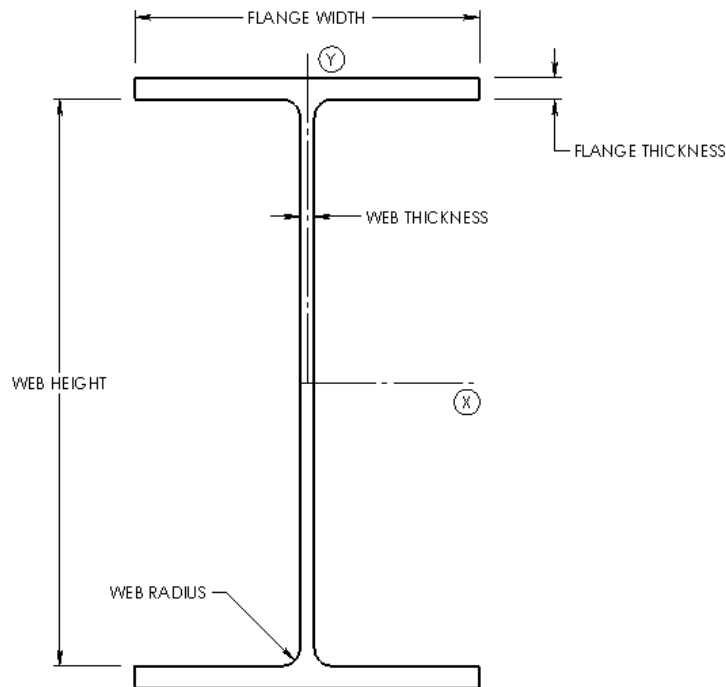


Figure A1.3 Reference of symmetric I-beam geometry

Cross-Sectional Area,
$$A = 2bt + dt_w + \frac{\pi * r_w^2}{4}$$
 Eq. (112)

Area Moment of Inertia,
$$I_x = \frac{b(d + 2t)^3}{12} - \frac{(b - t_w)d^3}{12}$$
 Eq. (113)

²⁵ For doubly-symmetric I-Beams.

Radius of Gyration,

$$r_x = \sqrt{\frac{I_x}{A}} \quad \text{Eq. (114)}$$

Elastic Section Modulus,

$$Z_{e,x} = \frac{I_x}{\bar{y}} \quad \text{Eq. (115)}$$

Torsional Stiffness Factor,

$$K = \frac{1}{2}(2t^3b + t_w^3d) \quad \text{Eq. (116)}$$

Warping Constant,

$$C_w = \frac{H^2tb^3}{24} \quad \text{Eq. (117)}$$

Plastic Section Modulus,

$$Z_{p,x} = \frac{t_w d^2}{4} + bt(d + b) \quad \text{Eq. (118)}$$

Shape Factor,

$$SF_x = \frac{Z_{p,x}\bar{y}}{I_x} \quad \text{Eq. (119)}$$

Area Moment of Inertia,

$$I_y = \frac{b^3t}{6} + \frac{t_w^3d}{12} \quad \text{Eq. (120)}$$

Radius of Gyration,

$$r_y = \sqrt{\frac{I_y}{A}} \quad \text{Eq. (121)}$$

Plastic Section Modulus,

$$Z_{p,y} = \frac{b^2t}{2} + \frac{t_w^2d}{4} \quad \text{Eq. (122)}$$

Elastic Section Modulus,

$$Z_{e,y} = \frac{I_y}{\bar{x}} \quad \text{Eq. (123)}$$

Shape Factor,

$$SF_y = \frac{Z_{p,y}\bar{x}}{I_y} \quad \text{Eq. (124)}$$

Polar Moment of Inertia,

$$J = I_x + I_y \quad \text{Eq. (125)}$$

Shear Modulus,

$$G = \frac{E}{2(1 + \nu)} \quad \text{Eq. (126)}$$

Results from these equations are shown in Table A1.2 on the following Page.

Table A1.2 Beam geometry calculation results

Section Dimensions		
Flange Width	5.75	in
Flange Thickness	0.36	in
Web Height	9.45	in
Web Thickness	0.24	in
Web Radius	0.30	in
Section Properties		
Area	6.48	in²
Centroid, y	5.09	in
Centroid, x	2.88	in
Total Height	10.17	in
(Area Moment of Inertia), x	116.53	in⁴
Radius of Gyration, x	4.24	in
Plastic Modulus, x	36.82	in³
Elastic Modulus, x	22.92	in³
Shape Factor, x	1.61	
(Area Moment of Inertia), y	11.42	in⁴
Radius of Gyration, y	1.33	in
Plastic Modulus, y	6.09	in³
Elastic Modulus, y	3.97	in³
Shape Factor, y	1.53	
Polar Moment of Inertia	127.94	in⁴
Torsional Constants		
k1	0.09	
k2	0.04	
α	0.23	
D	0.54	
K1	0.26	
K2	0.34	

APPENDIX B

IMPORTANT LOAD CONSIDERATIONS

B.1 Static Load Analysis

B.1.1 Centroid Analysis

Simple free-body diagrams can be employed to accurately²⁶ predict the center of gravity and reactions at different supports along the frame. The primary method is simply:

$$CoG(x, y, z) = \frac{\sum M_{z(x),z(y),x(z)}}{\sum Load} \quad \text{Eq. (127)}$$

B.2.2 Tire Load Analysis [50]

Given a calculated axle weight, the following calculations can be made to estimate the rolling resistance of the trailer (and ultimately the available drawbar pull) and the deflection in the trailer tires.

$$Load = \frac{W}{n_{tires}} \quad \text{Eq. (128)}$$

Where, W is in kilograms. The tire foot print width is given as:

$$W = 25.4s(1.03 - 0.004a) \quad \text{Eq. (129)}$$

Where, a is the tire aspect ratio and s (tire section width) is in millimeters. Calculate next, the tire section height (if not known).

$$h = \frac{sa}{25.4} \quad \text{Eq. (130)}$$

If s is known in inches, the equation is then simply: $h = sa$. The tangential stiffness is calculated as:

$$t = 0.002p\sqrt{-2.581W(D + 0.0008aW)(a - 257.5)} + 3.45 \quad \text{Eq. (131)}$$

Where, p is in pounds per square inch and total expected deflection is given as:

²⁶ The accuracy is respective of the reported weights of individual components either from the component manufacturer or computer software.

$$h' = 0.017858 \frac{Load}{t} \quad \text{Eq. (132)}$$

Finally, the coefficient of rolling resistance is calculated by:

$$C_{rr} = \frac{-0.01h'[p + 0.019(v^2 + 10526.3)]}{(h' - 2D)p} + \frac{0.000095(v^2 + 10526.3)}{p} + 0.005 \quad \text{Eq. (133)}$$

Where, v is the trailer velocity. The actual rolling resistance per tire is then,

$$RR = \frac{2.2046W C_{rr}}{4} \quad \text{Eq. (134)}$$

The available drawbar can then be calculated as:

$$DB = \frac{T_w}{r_{tire}} - RR \quad \text{Eq. (135)}$$

Where, T_w is the torque resolved at the tires and r_{tire} is the rolling tire radius.

B.1.3 Leaf Spring Deflection Analysis

Typically, springs are thought of as linear and are represented as,

$$F = kx \quad \text{Eq. (136)}$$

Where, k is the spring rate, F is the force applied and x is the linear displacement. This

mainframe design utilizes leaf springs, which due to their tapered design and variable cross-section exhibit a non-linear response and as described as progressive-rate springs. The following is a method for calculating leaf spring stress and deflection.

$$\delta = \frac{\delta_c qFL^3}{ENb_N h^3} \quad \text{Eq. (137)}$$

Where,

$$\delta_c = \frac{1 - 4m + 2m^2[1.5 - \ln(m)]}{(1 - m)^3} \quad \text{Eq. (138)}$$

Where, $q = 3$ and $m = N_f/N$ and N_f is the number of full leaves in the spring, N is the total number of leaves, E is the elastic modulus, h is the spring seat height and $b_N = b/N$; where, b is the spring width. Alternatively, there exist formulae for flat springs based on beam bending equations for cases of small deflection. One such equation is [51],

$$\delta = \frac{FL^3}{4Ebh^3} \quad \text{Eq. (139)}$$

These equations assume that the spring is loaded on its geometric axis of symmetry, which as we know from practice, is not always the case. Calculations with these equations showed an error of more than 10% for most of the data points provided from the manufacturer.

The following table shows published deflection verse load values for the leaf springs with a GAWR of 25,000lbs.

Table B1.1 Published leaf spring data

Load Per Spring (lbs)	Deflection (in)
0	0
2000	0.21
4000	0.42
6000	0.60
8000	0.78
10000	0.85
12000	1.07
14000	1.18
16000	1.31
18000	1.42
20000	1.53
22000	1.62

Based on the above table and calculated weights, the following equations were extrapolated to predict spring deflection. The results from these equations are to be compared with actual data and thereby validated.

$$\delta = 0.0004F^{0.8412} \quad \text{Eq. (140)}^{27}$$

$$\delta = -4 \times 10^{-18}F^4 + 2 \times 10^{-13}F^3 - 5 \times 10^{-9}F^2 + 0.0001F - 0.0043 \quad \text{Eq. (141)}^{28}$$

²⁷ $R^2 = 0.9947$, the average error is 5.33%, however, the error over the load range of interest is just 1.02%.

²⁸ $R^2 = 0.9986$, the average error is 3.99%, however, the error over the load range of interest is 2.65%.

APPENDIX C

INSTRUMENTATION

C.1 Strain Gauge Instrumentation

C.1.1 Concepts Bonded Wire Resistance Gauges

Bonded wire resistance strain gauges consist of some pattern of small wires to be attached to a material or object for strain testing. Any change in the surface area of the object will result in a similar, measurable change in the length and cross-section of strain gauge wiring. In the case of a beam, we are concerned with extension at the bottom edge and compression at the top edge of the material. An example of this is shown in following figure.

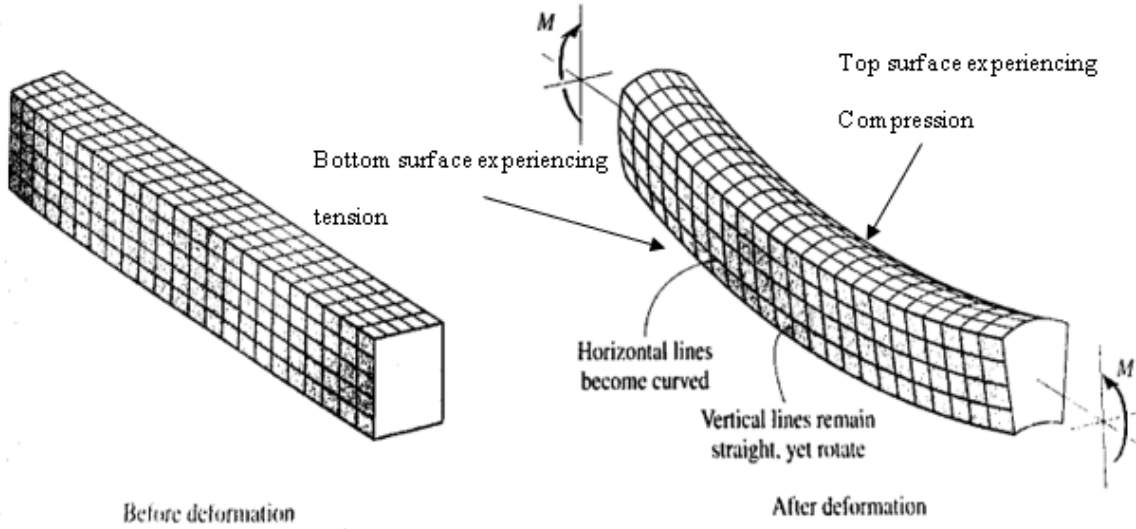


Figure C1.1 Deformations in a beam element [52]

This change will result in an electrical resistance change of the strain gauge. If the strain gauge were to be located on the underside of the beam, it would be placed under tension and the gauge resistance would increase. However, the strain gauge which is located on the top surface of the beam will experience the opposite effect. A standard device to measure change in resistivity is a Wheatstone bridge and if compared to the change in length one can determine a gauge factor for the strain gauge utilized. The gauge factor can be calculated as:

$$G.F. = \frac{\Delta R/R}{\Delta L/L} \quad \text{Eq. (142)}$$

In the above equation, R , L and $G.F.$ are resistance, length and gauge factor, respectively [53].

$\Delta L/L$ is the strain, ε , (unit length/unit length). With this definition, we can state the gauge factor simply as:

$$G.F. = \frac{\Delta R/R}{\varepsilon} \quad \text{Eq. (143)}^{29}$$

Because the change in resistance here is very small, the use of a Wheatstone bridge is very practical.

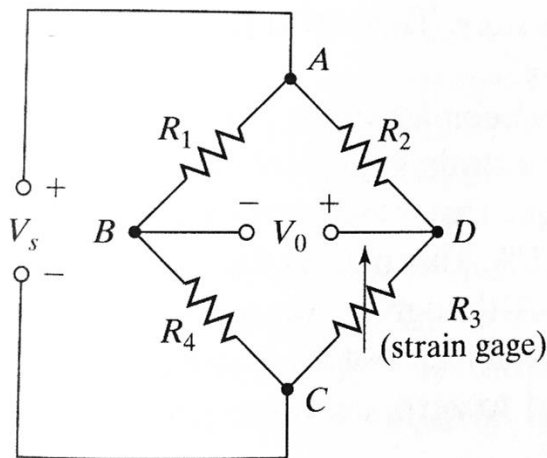


Figure C1.2 A constant voltage Wheatstone bridge

At the initial condition, one where the beam previously mentioned is unstrained, the value of all four resistors will be the same. Accordingly, the voltage at points B and D will be the

²⁹ It is important to note that there is, in some cases, appreciable error due to transverse strain across the gauge. There is then understandably, two gauge factors, and as such, this equation can be rewritten as: $\Delta R/R = G.F._a \varepsilon_a + G.F._t \varepsilon_t$, where the subscripts, a and t are axial and transverse directions, respectively.

same and therefore, the output voltage, V_o , will be zero. In this state, the bridge is considered to be balanced. As we begin applying a load, the strain gauge will begin to adjust and in turn affect the values of R_3 . As the values of R_3 begin to change, the voltage out will also begin to show variance from the initial condition. Therefore, we can assume that if the bridge was balanced initially, any change in gauge resistance will be proportional to the change in the voltage output of the circuit [54]. A variation of this is a Half-Bridge Wheatstone circuit as shown.

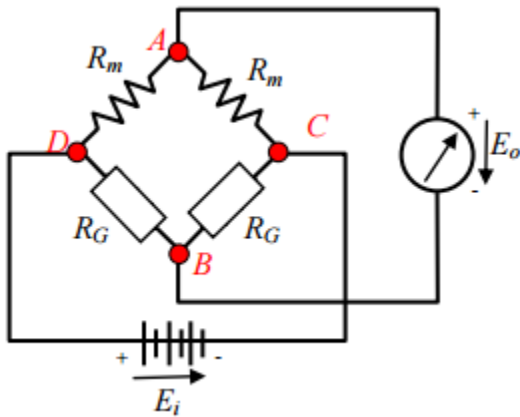


Figure C1.3 Wheatstone half-bridge circuit

Because this setup only contains two active resistors (as opposed to four in a Full-Bridge Wheatstone circuit), a signal conditioning device is required. This is to complete the bridge with reference resistors. These reference resistors are fixed and therefore ideal for detecting miniscule voltage changes across the circuit. The following figure shows the bridge completion of a Half-Bridge Wheatstone circuit.

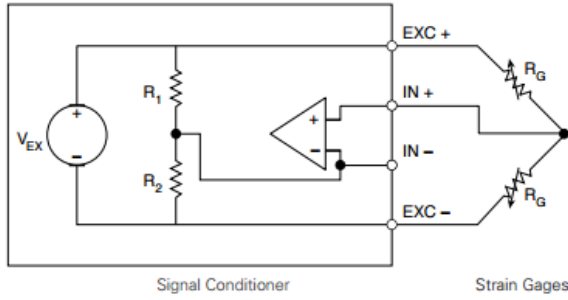


Figure C1.4 Bridge complete of a half-bridge Wheatstone circuit [55]

We can analyze this circuit and derive a method for relating the strain to the voltage output and gauge factor. Associating the resistance between junctions C and B with the gauge on the top surface of the beam and the resistance between junctions D and B corresponding with the strain gauge on the bottom surface of the beam, we can say that:

$$R_{CB} = R_{G0} + \Delta R = R_G(1 + G.F.* \varepsilon) \quad \text{Eq. (144)}$$

$$R_{DB} = R_{G0} - \Delta R = R_G(1 - G.F.* \varepsilon) \quad \text{Eq. (145)}$$

Where R_{G0} is the nominal unstrained resistance. In the figure on the previous page, R_m is the nominal resistance between junctions C and A as well as between junctions D and A. With that, we can then analyze the entire circuit and reduce it down to a more manageable form as shown.

$$\frac{E_0}{E_i} = \frac{R_m}{R_m + R_m} - \frac{R_G(1 - G.F.* \varepsilon)}{R_G(1 + G.F.* \varepsilon) + R_G(1 - G.F.* \varepsilon)} \quad \text{Eq. (146)}$$

$$\frac{E_0}{E_i} = \frac{G.F.* \varepsilon}{2} \quad \text{Eq. (147)}$$

We now have to consider a comparison of the circuit when it is strained verses unstrained. To do this, we will introduce, V_r , as the difference in voltage as the strain changes. If we define V_r as shown below [56], it follows that we can rearrange this relationship to a more beneficial form as shown.

$$V_r \equiv \left(\frac{E_0}{E_i}\right)_{Strained} - \left(\frac{E_0}{E_i}\right)_{Unstrained} \quad \text{Eq. (148)}$$

$$\varepsilon = \frac{-2V_r}{G \cdot F}. \quad \text{Eq. (149)}$$

Having solved for strain we can now calculate the stress, once again using Hooke's Law.

$$E = \frac{\sigma}{\varepsilon} \quad \text{Eq. (150)}$$

Having accomplished all of this, we can now compute the stiffness, k , of the element by comparing the ratio of the force applied to the deflection due to the load.

$$k = \frac{P}{v_p} \quad \text{Eq. (151)}$$

C.1.2 Placement of Strain Gauges

Once preliminary theoretical and mesh analysis are complete, one should have a good idea of where to place strain gauges to validate the analysis. High stresses in road going structures are typically found at welded joints and areas of beam bending. In case of beam bending, gauge placement is self-explanatory; however, to measure strain at a welded connection, one must first determine the likely failure initiation site. Typically, a weld will fail at the toe as this creates a notched stress concentration. For a calculation of fatigue life in these instances, see the section 2.2 Failure and Fatigue. Alternatively, if there is poor penetration of the weld material into the base material (see C1.5), failure through the cross section of the weld can occur.

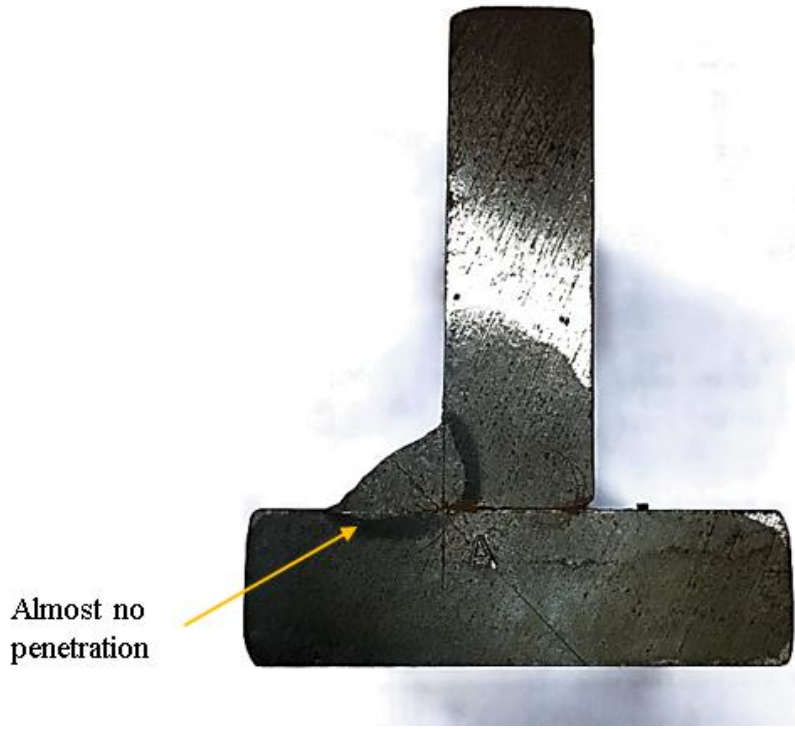


Figure C1.5 Example of poor welding

Strain gauges should be placed as close to the weld toe as surface preparation allows. A benefit of FEA is that often a stress tensor plot can be generated, such plots showing stress direction can be useful in placing strain gauges at the optimal orientation. The following figures are examples of well-placed strain gauges at the weld toe notch.



Figure C1.6 Sample strain gauge placement at weld toe

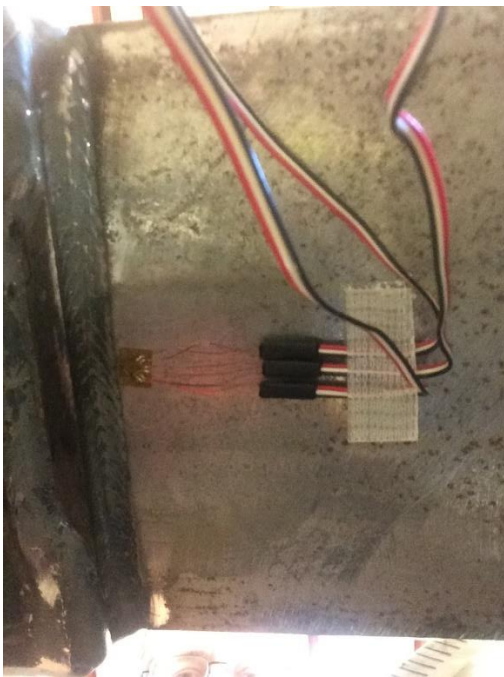


Figure C1.7 Sample strain gauge placement at weld toe

VITA

Daniel Landgraf was born in Camden, New Jersey; the youngest of three children. He graduated high school in 2006 from Central Bucks South High School in Bucks County, Pennsylvania. After graduation, Daniel joined the United States Army and served on active duty from July 2008 to February 2012 at which time he was honorably discharged. During his time on active duty, Daniel was stationed in Wiesbaden, Germany and deployed to Iraq in support of both Operations Iraqi Freedom and New Dawn. After leaving the active duty component, Daniel moved back to the United States, joined the Army National Guard and enrolled in college. Daniel completed his Associates of Applied Science degree in General Engineering Technology from Chattanooga State Community College in 2015 and two years later graduated from The University of Tennessee at Chattanooga (UTC) with a Bachelor of Science degree in Mechanical Engineering. Hired as a Mechanical Engineering Intern in May 2017, Daniel earned a full-time position at Sherman + Reilly, Inc in January 2018 and in addition to conducting research and analysis is responsible for the structural design of all machine trailers. Daniel is planning to graduate with a Master of Science degree in Mechanical Engineering from UTC in December 2019. Daniel's greatest aspiration is to lead a life of learning and to share his knowledge and experience with those around him.